A Neutron Flux Measurement System for ASDEX

G. Assi[+)], H. Rapp

IPP III/70 March 1981

MAX-PLANCK-INSTITUT FÜR PLASMAPHYSIK

8046 GARCHING BEI MÜNCHEN

MAX-PLANCK-INSTITUT FÜR PLASMAPHYSIK

GARCHING BEI MÜNCHEN

A Neutron Flux Measurement System for ASDEX

G. Assi[+], H. Rapp

IPP III/70 March 1981

[+] New address since January 1981:

Dr. Gianni Assi
European Patent Office
Directorate General 1

NL-2280 HV Rijswijk

Die nachstehende Arbeit wurde im Rahmen des Vertrages zwischen dem Max-Planck-Institut für Plasmaphysik und der Europäischen Atomgemeinschaft über die Zusammenarbeit auf dem Gebiete der Plasmaphysik durchgeführt.

IPP III/70

G. Assi
H. Rapp

A Neutron Flux Measurement System for ASDEX

March 1981

(in English)

Abstract

A neutron flux measurement system has been developed for evaluating the ion temperature in the ASDEX tokamak. The system uses ^{10}B or ^{3}He proportional counters for neutron detection. The results of computations and test measurements show the influence of several factors on the error for the ion temperature determination. Test measurements were made in the Wendelstein VII a stellarator the results being in good agreement with other diagnostics.

Table of Contents

		page
1.	Introduction	1
2.	Neutron detecting system	3
2.1	Detectors, moderator, shield	3
2.2	Electronics, noise	8
2.3	Calibration	10
3.	Computations	11
3.1	Neutron flux from a plasma torus	11
3.2	Ion temperature	16
3.3	Scattering and shielding effects	19
4.	Numerical results and measurements	23
4.1	Neutron flux	24
4.2	Test measurements in the W VIIa stellarator	29
5.	Uncertainties, errors	35
6.	Appendices	43
7.	References	60

1. Introduction

The difficulties involved in neutron flux measurement and determination of the ion temperature from it in a toroidal device are governed by several factors which can be attributed to three main causes.

The first is the geometry. The neutrons from a large-volume toroidal plasma create a complicated flux field. This field, moreover, is modulated by the heavy masses around the torus where neutrons are scattered and shielded.

The second is the plasma. Neutrons are created not only by fusion between deuterium ions but also by photo-disintegration processes and by gamma-induced processes at the limiter or the wall. Fusion reactions can occur in a Maxwellian plasma or between beam ions and bulk ions and between beam ions themselves.

The gamma flux can cause much noise in the detector, depending on its location on the torus. The intense neutron flux change, e.g. during neutral beam heating of the plasma, calls for equipment covering several magnitudes of flux with sufficient time resolution and tolerable error.

Thirdly, the common problems of measurement techniques have to be overcome. The most important point is calibration of the equipment. This is very much related to the geometry. Because the neutron flux only yields information on the volume-integrated plasma reactivity, one needs information on the density profile and an assumption on the normalized temperature profile for determining the ion temperature.

The main task of the neutron flux diagnostics in ASDEX is that it affords direct and prompt proof of the consistency of plasma parameters measured by other diagnostic equipment. If one is only interested in correlating some experimental events or measuring qualitative behavior some of the problems mentioned above will vanish.

2. Neutron detecting system

The detecting system is based on reactions between slow and epithermal neutrons and the isotopes ^{10}B and ^{3}He. The fast neutrons are slowed down by means of a wax moderator surrounding the counters. Any information on their energy is lost. The pulses from the proportional counter tube are uniform and correspond to the reaction energy. This fact allows the use of a single-channel analyzer (SCA), with suitable lower level and small window, to reduce electronic and electromagnetic noise or noise due to gamma radiation.

The principal arrangement for each detecting channel of different sensitivity or at different locations consists of the detector surrounded by the moderator, a shield to reduce the influence of scattered neutrons, and a preamplifier and an amplifier with a SCA (Fig. 1). The signals of up to four channels can be simultaneously recorded on a multi-channel analyzer (MCA) either in PHA mode (pulse-height analysis) for the proper setting of the amplifiers and SCAs, or in MCS mode (multi-channel scaling) for the scaling of the neutron flux. Alternatively, a CAMAC interface with an 8-channel scaler module and memory will be used, allowing data acquisition and evaluation of the plasma temperature by means of the ASDEX computer.

2.1 Detectors, moderator, shield

Two types of neutron detectors are used: the boron and the helium proportional counters, the former being filled with boron trifluoride (BF_3) gas which can be natural or highly enriched (up to 96 %) in boron-10, the latter with helium-3.

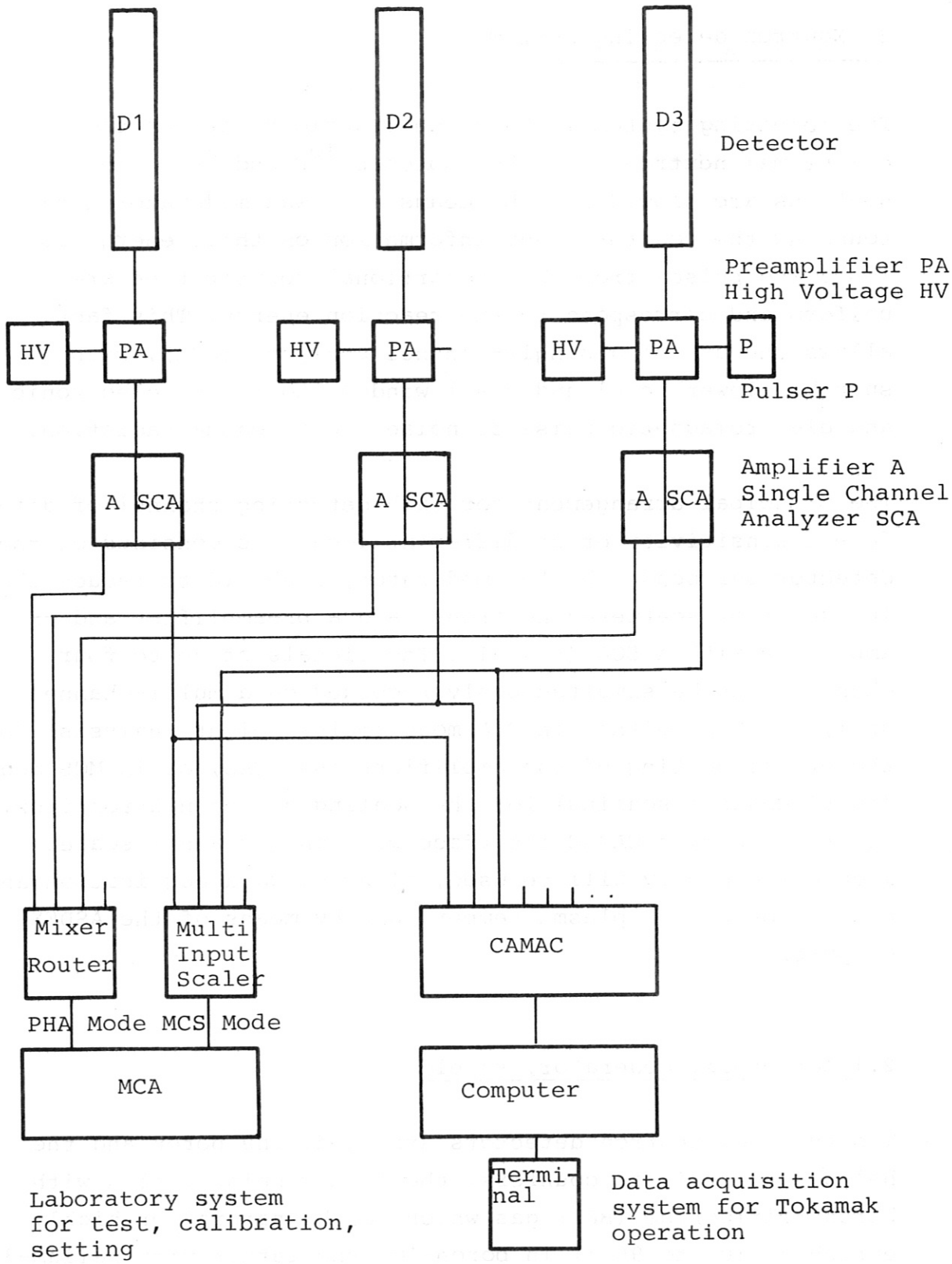

Fig. 1 Neutron flux measurement system

The reactions involved are /1/:

$$^{10}B + n \rightarrow {}^{7}Li + \alpha + 2.79\ MeV \quad (6.1\ \%)$$

$$^{10}B + n \rightarrow {}^{7}Li + \alpha + 2.31\ MeV \quad (93.9\ \%)$$

$$^{7}Li \rightarrow {}^{7}Li + \gamma + 0.478\ MeV$$

and

$$^{3}He + n \longrightarrow {}^{3}H + p + 0.764\ MeV$$

The cross-sections are shown in Fig. 2. According to the neutron energy dependence of these cross-sections, fast neutrons must first be moderated in order to be detected with higher efficiency. The simplest way to do this is to put a boron or helium counter inside a cylindrical paraffin moderator. By this means the neutron detection efficiency is nearly independent of the neutron energy over a wide range. A sketch of this arrangement is given in Fig. 3. Bars made of polythylene and detector tubes can be placed in the central region of the moderator. By varying the type of the detector and its position within the moderator, it is possible to change its neutron sensitivity. The measuring accuracy can be improved by using a sheet of cadmium around the moderator. This captures the scattered neutrons not coming straight from the neutron source. In conjunction with a shield this yields a sensitivity pattern which is clearly enhanced in the forward direction.

To meet the wide range of several orders of magnitude for the neutron flux generated by a big tokamak, we used several detectors with different sensitivities. Each detector, i.e. counting channel, has an upper and lower count rate limit. The upper limit is given by pulse height degradation which

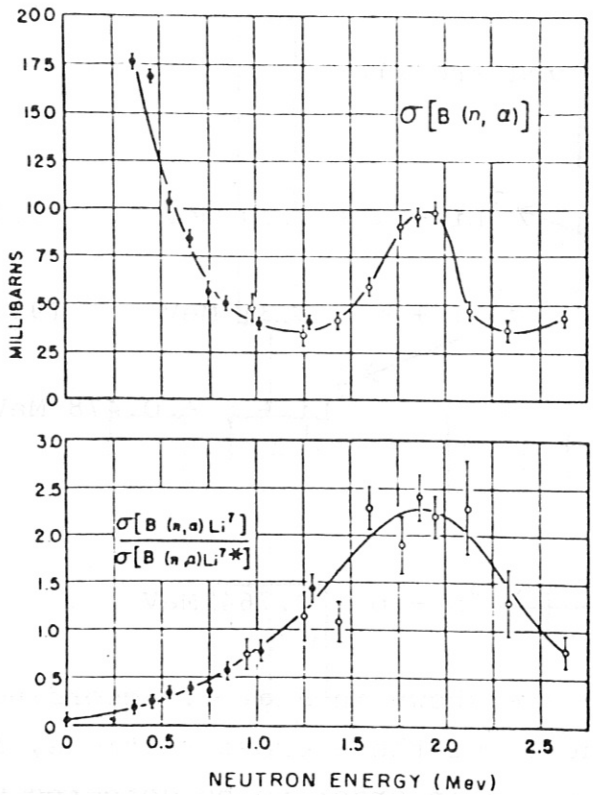

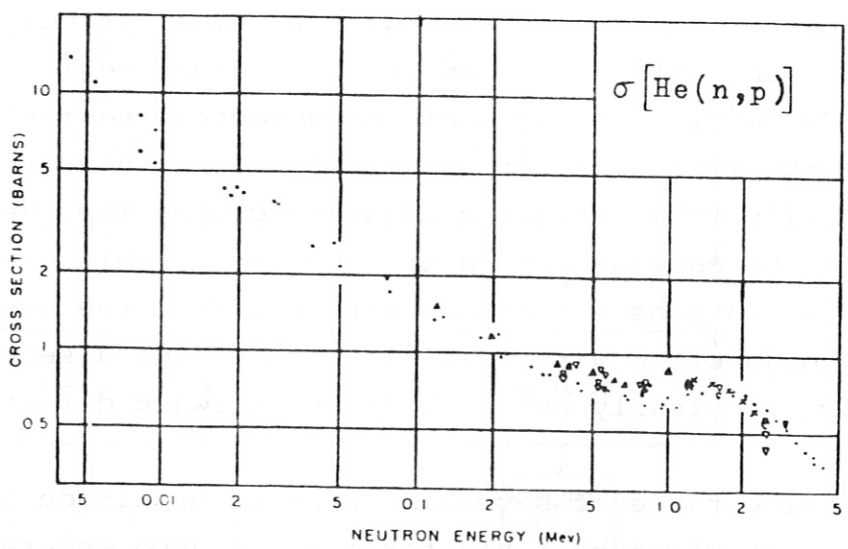

Fig. 2 Cross-sections for neutron detection /1;7/.

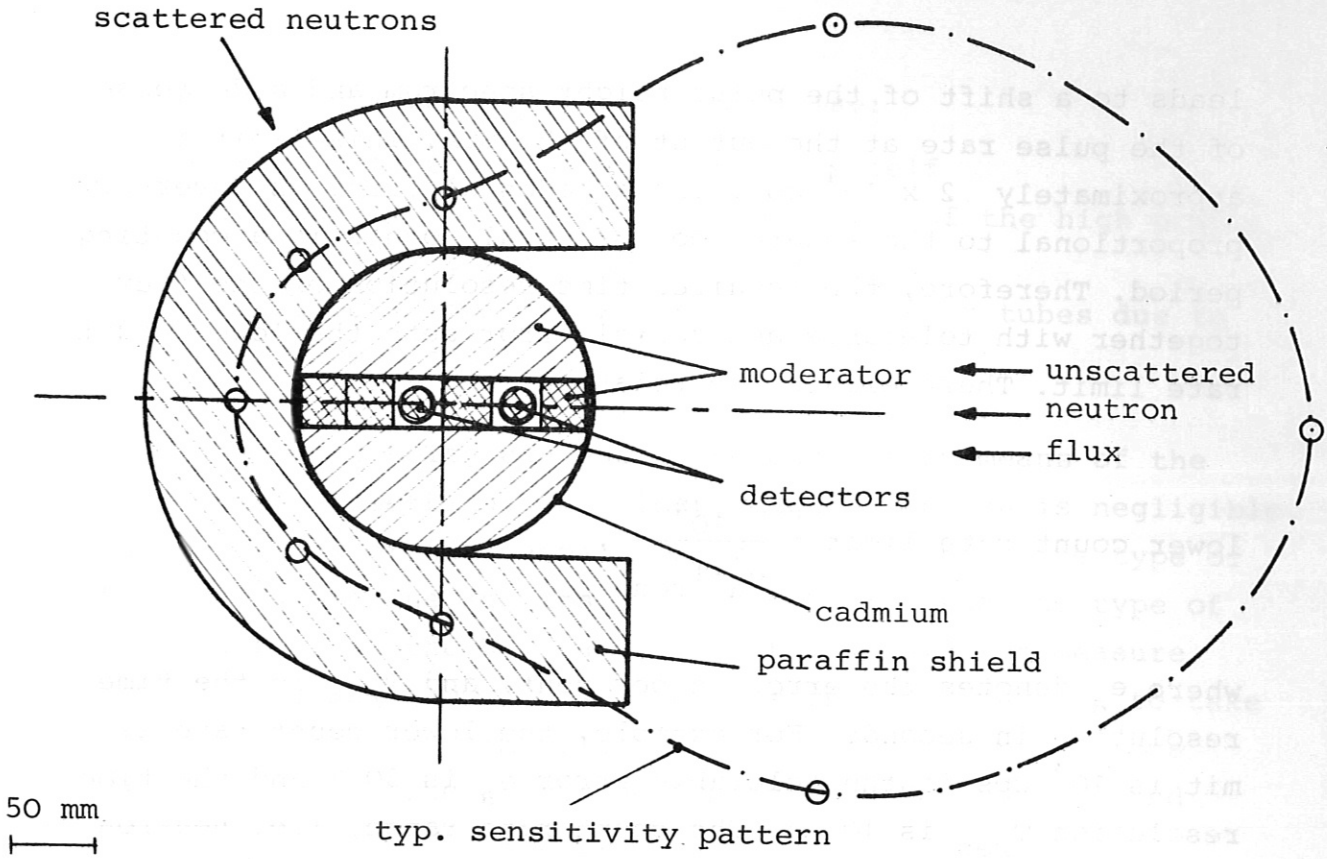

Fig. 3 Arrangement of detector, moderator and shield.

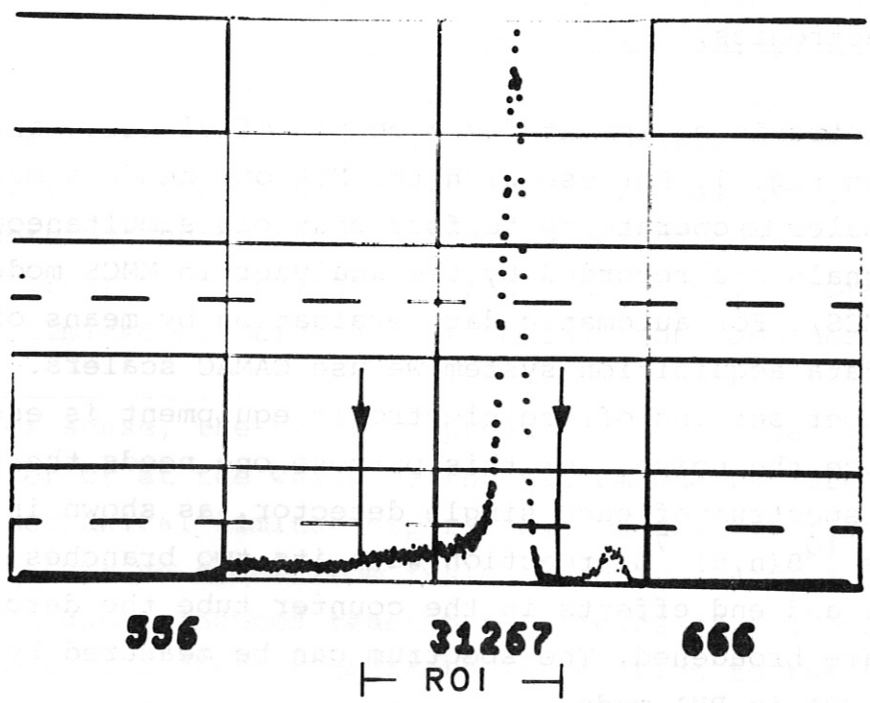

Fig. 4 Pulse height distribution for the $^{10}B(n,\alpha)^{7}Li$ reaction

leads to a shift of the pulse height spectrum and a decrease of the pulse rate at the output of the SCA. This limit is approximately 2×10^4 cps. The accidental error is inversely proportional to the square root of total counts in a counting period. Therefore, the required time resolution of the flux together with tolerable accidental error sets the lower count rate limit. There exists the relation

$$\text{lower count rate limit} = \frac{10^4}{e_a^2 \cdot T_{res}} ,$$

where e_a denotes the error in per cent, and T_{res} is the time resolution in seconds. For example, the lower count rate limit is 10^3 cps if the tolerable error e_a is 30 % and the time resolution T_{res} is 10 ms. The count rate range, i.e. neutron flux range, which can be measured by a single detector is therefore typically limited to one order of magnitude.

2.2 Electronics, noise

The electronic equipment for a couple of signal channels is shown in Fig. 1. For use with the MCA one needs a multi-input multiscaler to operate up to four channels simultaneously. The SCA signals are recorded by the analyzer in MMCS mode (multi-input MCS). For automatic data evaluation by means of the ASDEX data acquisition system we use CAMAC scalers.
The proper setting of the electronic equipment is essential to reduce the noise. For this purpose one needs the pulse height spectrum of each single detector, as shown in Fig. 4 for the $^{10}B(n,\alpha)\,^{7}Li$ reaction with its two branches. Owing to wall and end effects in the counter tube the descrete lines are broadened. The spectrum can be measured by means of the MCA in PHA mode.

There exist several sources of the noise:

- electronic noise from the equipment itself
- electromagnetic noise due to interaction of the high power electric circuits with the signal circuits
- photoelectrons from the walls of the counter tubes due to intense gamma radiation.

The electronic noise can easily be cut off by means of the discriminator setting. The electromagnetic noise is negligible. The magnitude of the gamma noise depends on both the type of the plasma machine and its operation regime and the type of the counter. In the W VIIa stellerator we did not measure any significant gamma noise, whereas in ASDEX we have to take care of this. The gamma flux can exceed 1 R/h or even one magnitude more. These are the limits for ^{3}He counters and ^{10}B counters, respectively.

To improve the signal-to-noise ratio, one can define a region of interest (ROI) of the spectrum (see Fig. 4). By means of a pulser the SCA window can be set to match the ROI. Only pulses in the ROI are then counted. For ^{3}He detectors we measured a decrease of the gamma noise by a factor of 6 if we used the SCA window instead of simple lower-level discrimination. In contrast, the improvement for BF_3 counters was negligible. It is therefore better to set the ROI for BF_3 counters rather broad in order to raise the tolerable upper count rate level, which is limited by pulse height degradation (see Sec. 2.1).

In a wider sense, the neutrons produced by γ-n reactions at the limiter or at the walls of the vacuum chamber are noise, too. In mechanical limiter experiments one can discriminate between volume neutrons from fusion reactions and wall neutrons from gamma-induced reactions by means of a proper arrangement of different counters in relation to the torus geometry /10/. In the case of a magnetic limiter experiment like

ASDEX this method may fail. Here the γ-n reactions can occur along the circumference of the torus. The intensity at different places widely varies according to location, depending only on the more or less accidental impingement of runaway electrons on the structure materials.

For this reason, shots with high gamma flux are not suitable for the neutron detecting equipment described here.

2.3 Calibration

The sensitivity of each channel was experimentally determined by means of a calibrated ^{238}Pu - B (α,n) neutron source the intensity of which is 6.8×10^6 n s^{-1} $\pm$ 3 %. The measurements were made in a small laboratory for comparison between different detector configurations and in the ASDEX experimental hall for absolute calibration. From this we learned the necessity of shielding against backscattered neutrons from the walls or neighbouring large masses. The contribution of the scattered neutrons not coming straight from the source to the measured signal can make calibration highly unreliable.

One of the main reasons for the error in neutron detector calibration is the large volume of the toroidal neutron emitting plasma relative to that of the very small, point-like neutron source. Moreover, the plasma is in a thick-walled vacuum chamber and is encircled by large copper coils, which causes neutrons to be scattered and shielded. We therefore moved the neutron source on the major radius of the plasma and measured the count rates as a function of the toroidal angle. This function is important for computational evaluation of the results, which is described in Sec. 3. A detailed study of the possible error is presented in Sec. 5.

3. Computations

In this section some computations are presented. They are related to the neutron flux produced by a toroidal device, to the time dependence of the ion temperature, and to the corrections that must be made to take into account the shielding effect due to materials between the plasma source and the detecting system.

3.1 Neutron flux from a plasma torus

At first the time dependence is not considered; it is also supposed that the shielding effect of the experimental arrangement is negligible. The plasma is considered as a large-volume, isotropically emitting neutron source. With reference to Fig. 5, the neutron flux in a point D (detection point) is given by the integral over the toroidal plasma volume V_p of all the elementary fluxes generated in D by the point-like sources S (source point) inside V_p:

$$\Phi_n(D) = \int_{Vp} d\Phi_{n,s}(D) = \int_{Vp} \frac{dn_s}{4\pi \cdot DS^2}, \tag{1}$$

where Φ_n is the neutron flux, $d\Phi_{n,s}$ the elementary flux, and dn_s is the number of neutrons generated per second inside a volume element dV_p situated in S; dn_s is given by the following expression:

$$dn_s = \tilde{R}(T,n)\, dV_p, \tag{2}$$

where T and n are the ion temperature and density; they are functions of the variable r = SC; $\tilde{R}(T,n)$ is the reaction rate

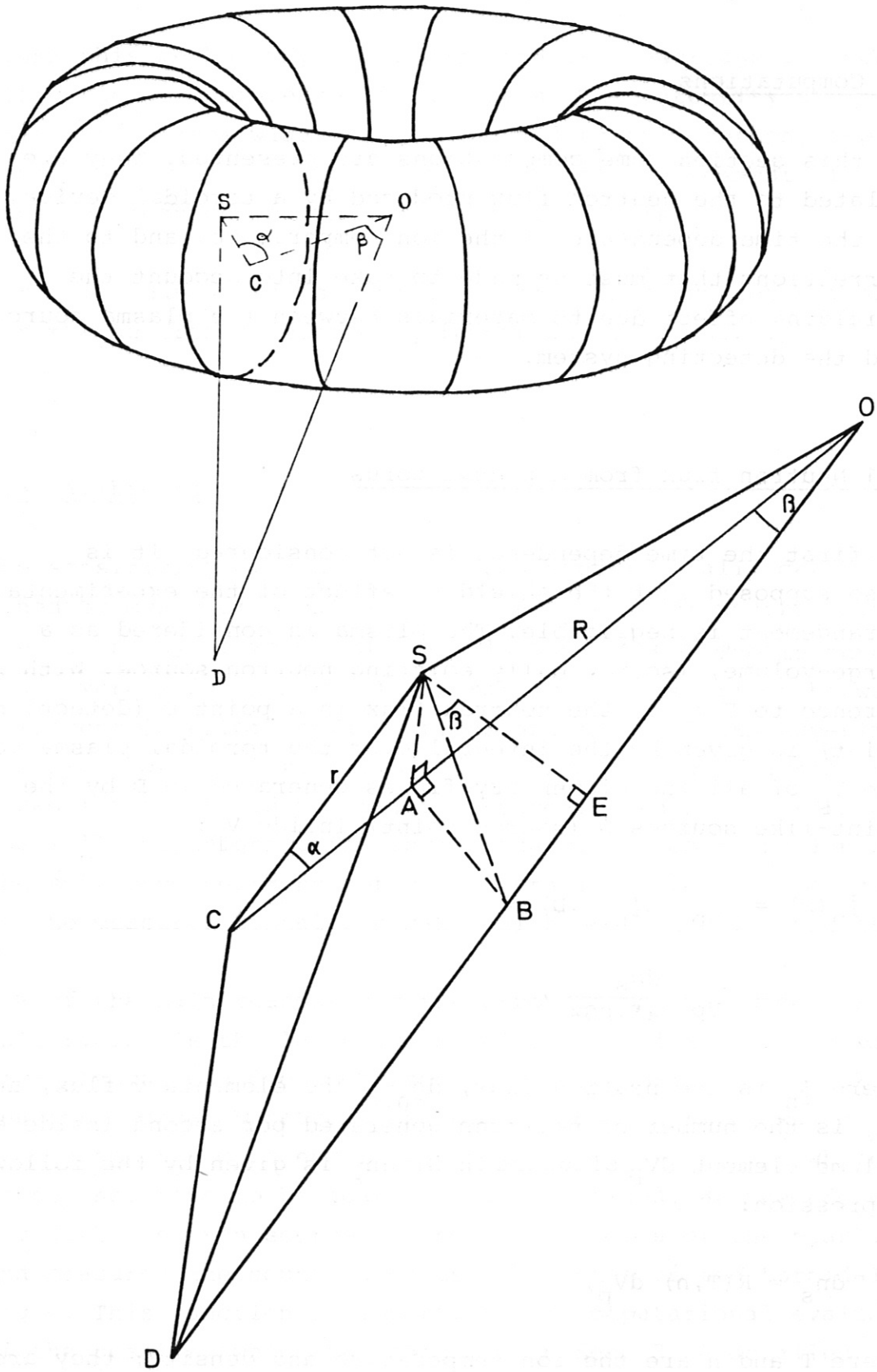

Fig. 5 Geometry for flux calculation. The triangle OCD lies in the mid plane of the torus.

of the plasma, i.e. the number of fusion reactions which take place per second inside a unit volume of plasma. Referring to a Maxwellian plasma and to D-D reactions, neutron branch, one has

$$\tilde{R}(T,n) = \frac{1}{2} n^2(r) \overline{\sigma V}(T(r)), \tag{3}$$

where $\overline{\sigma V}$ denotes the average value of the product between the deuteron velocity and the reaction cross-section, by computing the average over a Maxwellian distribution of velocities. The Gamow equation gives the expression of $\overline{\sigma V}$ /8/:

$$\overline{\sigma V}(T) = a_1 T^{-2/3} \exp(-a_2 T^{-1/3}). \tag{4}$$

The plot of $\overline{\sigma V}(T)$ is shown in Fig. 6. The space profiles $T(r)$ and $n(r)$ are assumed to be known; they depend on the particular toroidal device that produces the neutron flux. The volume element of the plasma torus is

$$dV_p = r(R-r\cos\alpha)dr\, d\alpha\, d\beta, \tag{5}$$

R being the mean torus radius (major plasma radius). By simple geometrical consideration DS^2 can be computed as a function of the coordinates r, α, β.
With reference to Fig. 5, one has

$$SB^2 = r^2\sin^2\alpha + (R-r\cos\alpha)^2 tg^2\beta, \tag{6}$$

$$BE = /SB \sin\beta/, \tag{7}$$

$$DE = R + a + d - \frac{R-r\cos\alpha}{\cos\beta} + BE, \tag{8}$$

and finally

$$DS^2 = SB^2 \cdot \cos^2\beta + DE^2, \tag{9}$$

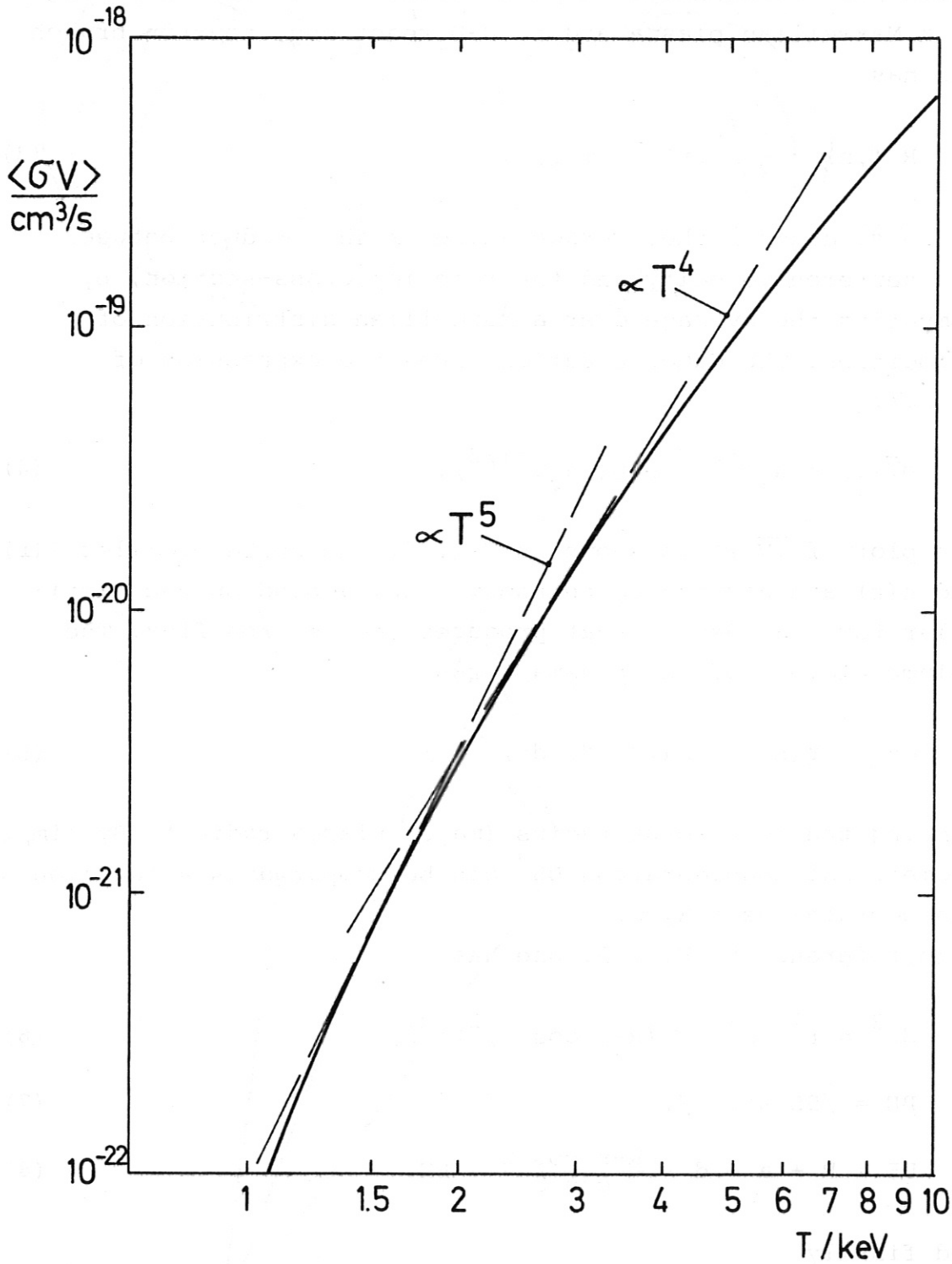

Fig. 6 $\overline{\sigma v}(T)$ for 3-dimensional Maxwellian ion distribution /6/.

where a is the minor radius of the plasma, and d is the distance between the detection point D and the surface of the plasma.

From relations (1) to (9) it follows that

$$\Phi_n(D) = \int_0^a dr \int_0^{2\pi} d\alpha \int_{-\pi}^{\pi} d\beta \frac{\tilde{R}(T(r),n(r))\, r(R-r\cos\alpha)}{4\pi^2 DS^2(r,\alpha,\beta)} \qquad (10)$$

If $d \gg 2a$, it is possible to give an approximate expression for the neutron flux. In fact, under this condition the toroidal plasma volume can be considered as a line (a circumference of radius R) that emits neutrons homogeneously and isotopically. With reference to Fig. 7, the neutron flux is

$$\Phi_n(D) = \int_{Lp} d\Phi_{n,\bar{S}}(D) = \int_{Lp} \frac{dn_{\bar{S}}}{4\pi D\bar{S}^2} \,. \qquad (11)$$

The integration is now done over the circumference L_p of radius R. The integrand has a similar meaning to that in eq. (1). In particular, $dn_{\bar{S}}$ is the number of neutrons generated per second inside a line element dL_p situated in $\bar{S}$. If n_{tot} is the total number of neutrons generated per second by the whole plasma, we get

$$n_{tot} = \int_{Vp} \tilde{R}(T(r),n(r))\, dV_p$$

$$= 2\pi \int_0^a dr \int_0^{2\pi} d\alpha\, \tilde{R}(T(r),n(r))\, r(R-r\cos\alpha) \qquad (12)$$

and hence

$$dn_{\bar{S}} = \frac{n_{tot}}{2\pi R} dL_p = \frac{n_{tot}}{2\pi} d\beta \qquad (13)$$

because $dL_p = Rd\beta$.

Since $\bar{d} = d + a$ and

$$D\bar{S}^2 = (\bar{d}+R)^2 + R^2 - 2\cdot(\bar{d}+R)\, R\cos\beta \qquad (14)$$

the final expression for the flux is

$$\Phi_n(D) = \int_{-\pi}^{\pi} \frac{n_{tot}}{8\pi^2 D\bar{S}^2(\beta)} \, d\beta. \qquad (15)$$

Some details about the numerical evaluation of integrals (10) and (15) can be found in Appendix 1.

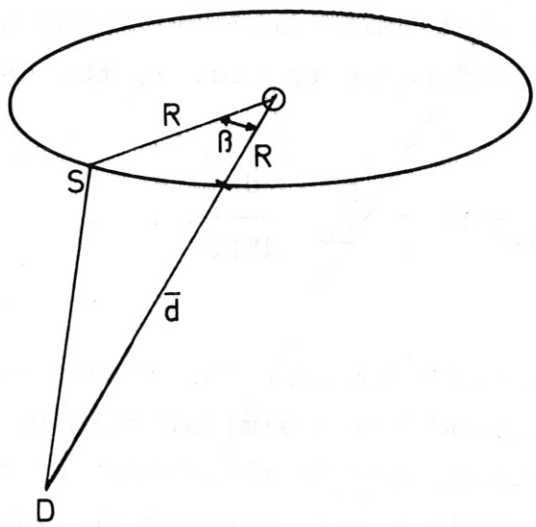

Fig. 7 Approximate model of the torus geometry when the detector is far off the plasma (distance between detector and plasma ≫ plasma radius)

3.2 Ion temperature

Still neglecting the shielding effect, we now take into account the time dependence of the ion temperature and density. The following expressions are considered:

$$T(r,t) = T_o(t) \cdot T(r);$$
$$n(r,t) = n_o(t) \cdot n(r);$$

where $T_o(t)$ and $n_o(t)$ give the time evolution of the central values (r = O) of T and n; T(r) and n(r) are normalized, i.e.

$$T(O) = 1,$$
$$n(O) = 1.$$

The neutron flux is now time dependent, too. Its exact expression is

$$\Phi_n(D,t) = \int_o^a dr \int_o^{2\pi} d\alpha \int_{-\pi}^{\pi} d\beta \cdot H \cdot r\,(R - r \cdot \cos\alpha) \qquad (18)$$

$$\text{with} \quad H = \frac{R(T(r,t),\, n(r,t))}{4\pi^2 DS^2(r,\alpha,\beta)}\,, \qquad (18\,a)$$

and the approximate one

$$\Phi_n(D,t) = \int_{-\pi}^{\pi} d\beta \cdot \frac{n_{tot}(t)}{8\pi^2 D\bar{S}^2(\beta)}\,. \qquad (19)$$

These expressions can be related to the output data of the experimental detecting system. This output usually takes the form of a histogram giving the number of counts f_i that have

been registered during each time interval $[t_i, t_i + \Delta t_i]$, for $i = 1, 2, 3, \ldots$. Only to fix a convention, the value f_i is referred to the time $t_i + \Delta t_i$ and, in such a way, the set of known points $(t_i + \Delta t_i, f_i)$ defines a function $f(t)$. The count rate $f_i/\Delta t_i$ is related to the time $t_i + \Delta t_i$, too, and can be computed by considering the neutron flux. If ε is the total efficiency, which has been defined as the count rate per unit incident flux, the following relation is valid:

$$\frac{f_i}{\Delta t_i} = \varepsilon \cdot \phi_n \, (D, t_i + \Delta t_i) \quad i = 1, 2, \ldots, \tag{20}$$

where $\Phi_n(D, t_i + \Delta t_i)$ is computed by means of eq. (18) or (19), and ε is experimentally determined. The functions $n_o(t)$, $n(r)$ are known because they are the output data of other diagnostics. The normalized radial dependence of the temperature $T(r)$ must be assumed as likely or arbitrary, e.g. as a parabolic function. In conclusion, relation (20) represents a set of equations whose solutions are

$$T_o(t_i + \Delta t_i) = T_{o,i}, \quad i = 1, 2, \ldots \tag{21}$$

The set of points $(t_i + \Delta t_i, T_{o,i})$ is then plotted and the graph of the function $T_o(t)$ is finally obtained. The solutions $T_{o,i}$ of eq. (20) can be found by looking for the zero point of the function

$$F(T_{o,i}) = \varepsilon \Phi_n(D, t_i + \Delta t_i) - \frac{f_i}{\Delta t_i} . \tag{22}$$

This method is advantageous if the integral Φ_n is first reduced to a simple summation by means of numerical analysis, and a computer is then used. Some details about the numerical solution of the equation $F(T_{o,i}) = 0$ can be found in Appendix 2.

3.3 Scattering and shielding effects

Between the neutron-emitting plasma and the detecting system the materials of the toroidal machine are placed: mainly the vacuum vessel and the toroidal field coils. Because of scattering processes and absorptions the neutron flux that reaches the detecting system is varied. Till now all the computations have been made on the assumption that such a variation is negligible. This assumption is now removed and the formulas obtained above are consequently corrected.

The plasma source is first simulated by means of a ^{238}Pu-B neutron source that is placed at different positions $\bar{S}$ inside the vacuum vessel along the circumference of radius R: see Fig. 8. The count rate, which is experimentally measured, is called $c_D(\beta)$. It depends on the detection site, i.e. the angle β. Moreover, $c_D(\beta)$ is influenced by the shielding effect of the materials between the plasma and D (see Fig. 12).

The count rate in D can also be theoretically computed under the hypothesis that there is no shielding effect at all. If q is the number of neutrons that are isotropically emitted by the source in $\bar{S}$, and ε is the efficiency of the detecting system, the theoretical count rate $C_{D,th}(\beta)$ without any shielding is given by

$$C_{D,th}(\beta) = \varepsilon \cdot \frac{q}{4\pi\, D\bar{S}^2(\beta)} \qquad (23)$$

The following function is then defined:

$$S(\beta) = \frac{C_D(\beta)}{C_{D,th}(\beta)} \cdot \qquad (24)$$

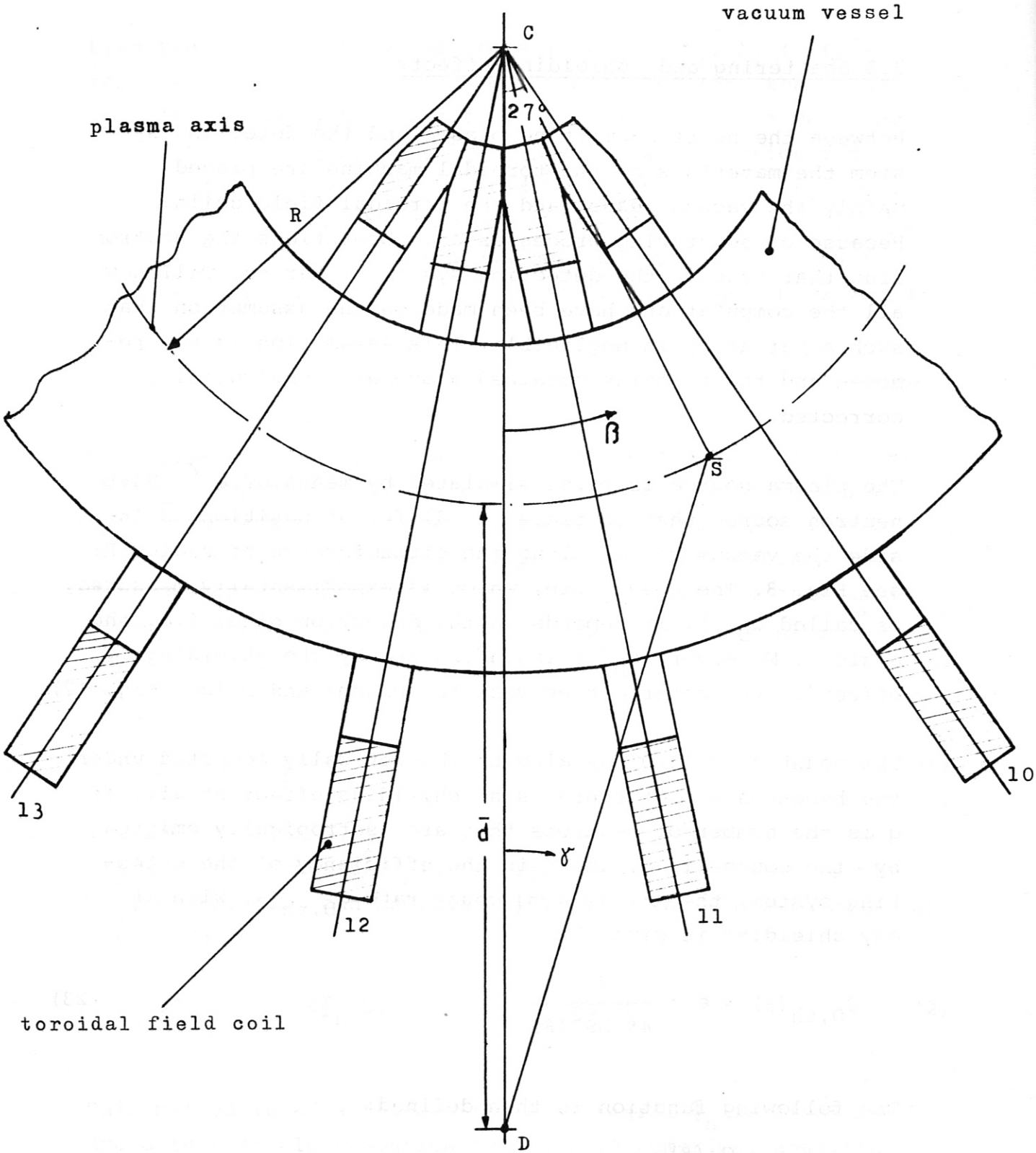

Fig. 8 Actual geometry of ASDEX tokamak. ß: toroidal angle of calibration source position $\bar{S}$. γ: viewing angle of neutron detector D.

With eq. (23) it follows that

$$S(\beta) = \frac{4\pi \; C_D(\beta) \cdot \bar{DS}^2(\beta)}{\varepsilon \cdot q} \; . \tag{25}$$

The function $S(\beta)$ is used as a correcting factor in the neutron flux computations. To be more precise, the plasma is again considered as a neutron source that produces a flux whose analytical expression is eq. (18). The product of ε and the function H (eq. (18 a) is the theoretical count rate in D due to a point-like plasma source in S of unit volume. According to eq. (24) and (25), the real count rate per unit volume is

$$\begin{aligned} C_{D,P}(\beta) &= \varepsilon \cdot \frac{\tilde{R}(T,n)}{4\pi DS^2(r,\alpha,\beta)} \cdot S(\beta) \\ &= \frac{\tilde{R}(T,n) \cdot C_D(\beta) \cdot D\bar{S}^2(\beta)}{q \cdot DS^2(r,\alpha,\beta)} \; , \end{aligned} \tag{26}$$

where DS^2 and $D\bar{S}^2$ are given by eqs. (9) and (14), respectively.

Equation (26) uses the implicit assumption that the same correcting factor $S(\beta)$ must be used for all the points that have the same β as $\bar{S}$ but different coordinates r and α. The real flux is then

$$\Phi_n(D,t) = \int_0^a dr \int_0^{2\pi} d\alpha \int_{-\pi}^{\pi} d\beta \cdot$$

$$\cdot \frac{\tilde{R}(T(r,t),n(r,t)) \, C_D(\beta) D\bar{S}^2(\beta) r(R - r\cos\alpha)}{\varepsilon q \; D\bar{S}^2(r,\alpha,\beta)} \; . \tag{27}$$

This assumption can be avoided if the approximate expression for the neutron flux (eq. (19)) is used. In this case, because the dependence on r and α no longer exists, the equality

$$DS^2(\beta) = D\bar{S}^2(\beta). \tag{28}$$

is valid, and the following expression of the flux can be proved:

$$\Phi_n(D,t) = \int_{-\P}^{\P} d\beta \; \frac{n_{tot}(t) C_D(\beta)}{2\P\varepsilon q} \; . \tag{29}$$

These new expressions (27) and (29) for the flux have to be used in the equation

$$F(T_{o,i}) = 0$$

(see eq. (22)) to compute the time function of the ion temperature.

Some details about the numerical determination of the function $S(\beta)$ with reference to a particular toroidal machine (ASDEX tokamak) can be found in Appendix 3.

4. Numerical results and measurements

The input data necessary for the computations are as follows:

a) ASDEX tokamak

Major plasma radius $R = 164$ cm
Plasma radius $a = 40$ cm
Normalized profiles

$$n_{(r)} = T_{(r)} = (1 - (\frac{r}{a})^2)^2 .$$

b) W VIIa stellarator

Major plasma radius $R = 200$ cm
Normalizing radius of the plasma $a_{FWHM} = 3$ cm
Normalized profiles

$$n_{(r)} = T_{(r)} = \frac{1}{1 + (\frac{r}{a_{FWHM}})^3} .$$

The upper limit for integration: $a = 10$ cm.
Maximum ion density as a function of time: see Figs. 13 a,b.

The detecting system is set up as shown in Fig. 3. It is placed between two contiguous toroidal field coils. The counter efficiency ε is 11 cps/nv for the ^{3}He counter and 0.12 cps/nv for the ^{10}B counter. For the test measurements in the stellarator, the distance between the plasma surface and the detector was $d = 118$ cm.

4.1 Neutron flux

The normalized reactivity versus the normalized radius for an ohmically heated deuterium plasma in ASDEX is shown in Fig. 9. The FWHM value gives good information on the effective radius of the plasma region where most of the fusion reactions take place.

The plots of the neutron flux versus the distance d between the plasma surface and the point in which the flux is computed can be seen in Figs. 10 and 11 for ASDEX and W VIIa, respectively. The flux is computed according to eq. (10) (exact solution) and eq. (15) (approximate solution) by means of the C.FLUXED and C.FLUXAD computer codes. For $d \to \infty$ it is quite obvious that both solutions coincide. The difference between them is greater for ASDEX than for W VIIa because the aspect ratio R/a is only 4 for ASDEX and 20 for W VIIa. In the range of distance d where the measuring equipment can normally be placed the flux variation due to variation of d is rather low. The error due to the value of d will thus be low, too. From the relation of the exact and approximate solution we can calculate a correction factor which depends only weakly on the distance d for values of $d \geq 1.5$ m. By this means we can use the approximate formula for the evaluation of the ion temperature with the same accuracy as the exact solution eq. (10).

The measured and calculated count rates as a function of the toroidal angle β are shown in Fig. 12 for ASDEX. The calucla-ted count rate $C_{D,th}(\beta)$ does not include any scattering or shielding effects due to coils etc. It is computed by the B.FIT code. The count rate C_D (β) was measured by means of the neutron source. It includes the sensitivity pattern of the

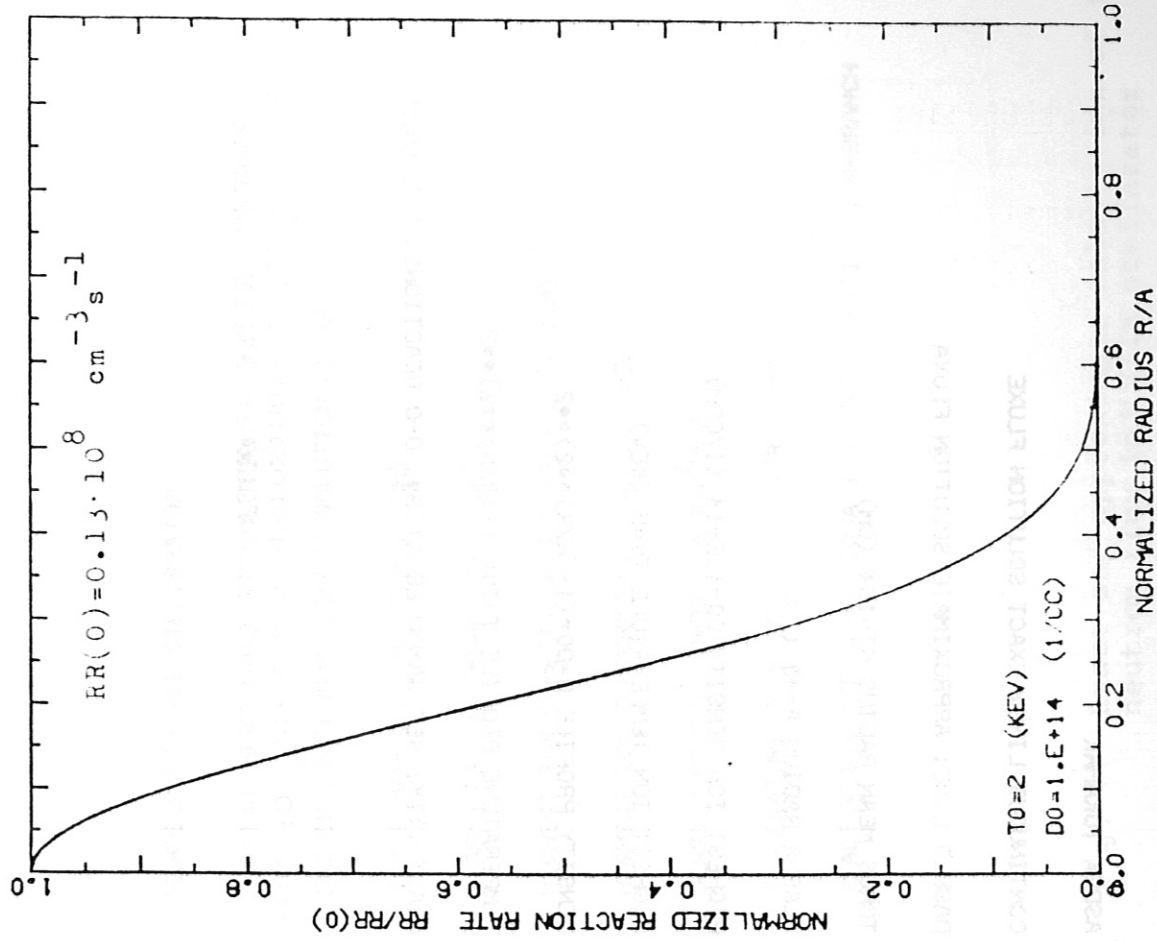

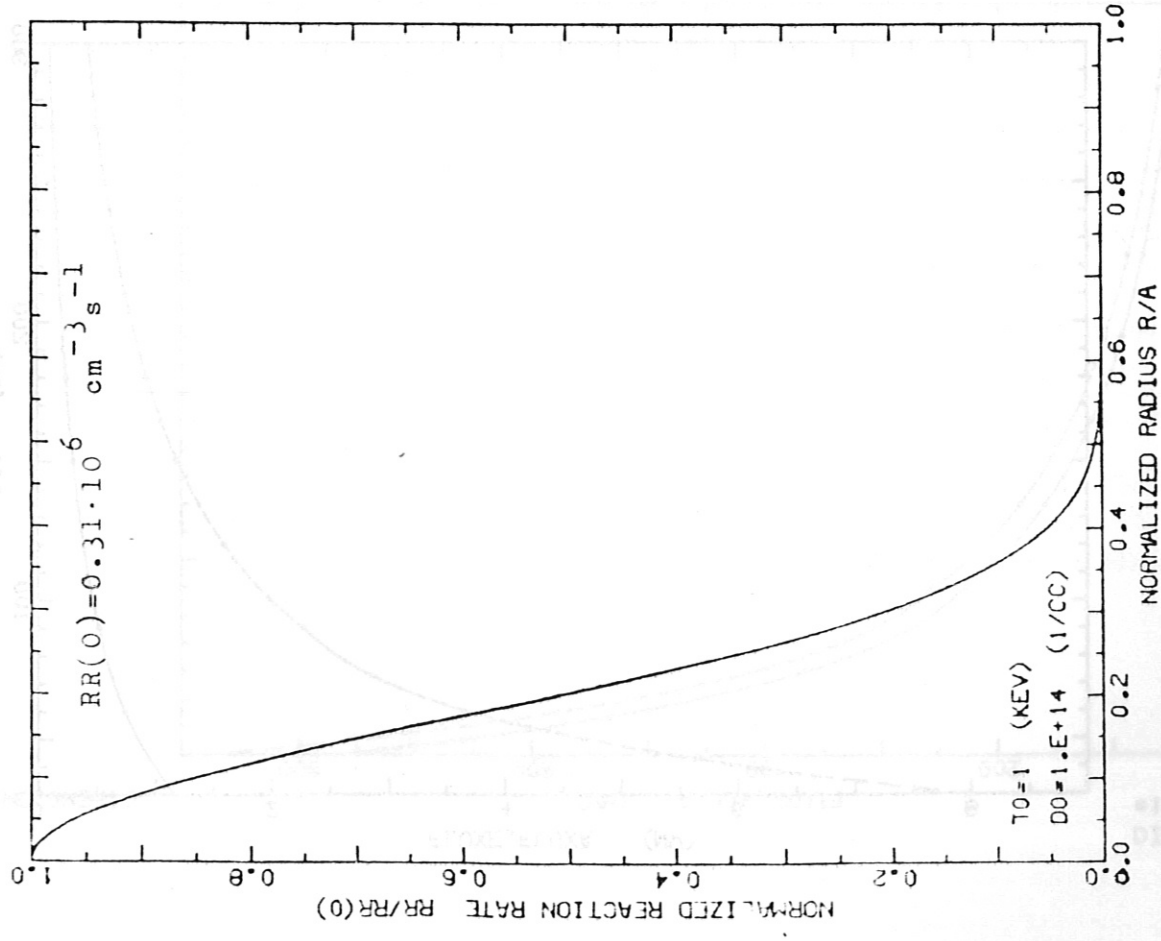

Fig. 9 The normalized reaction rate in ASDEX for T_i = 1 and 2 keV and maximum ion density of 10^{14} cm^{-3}.

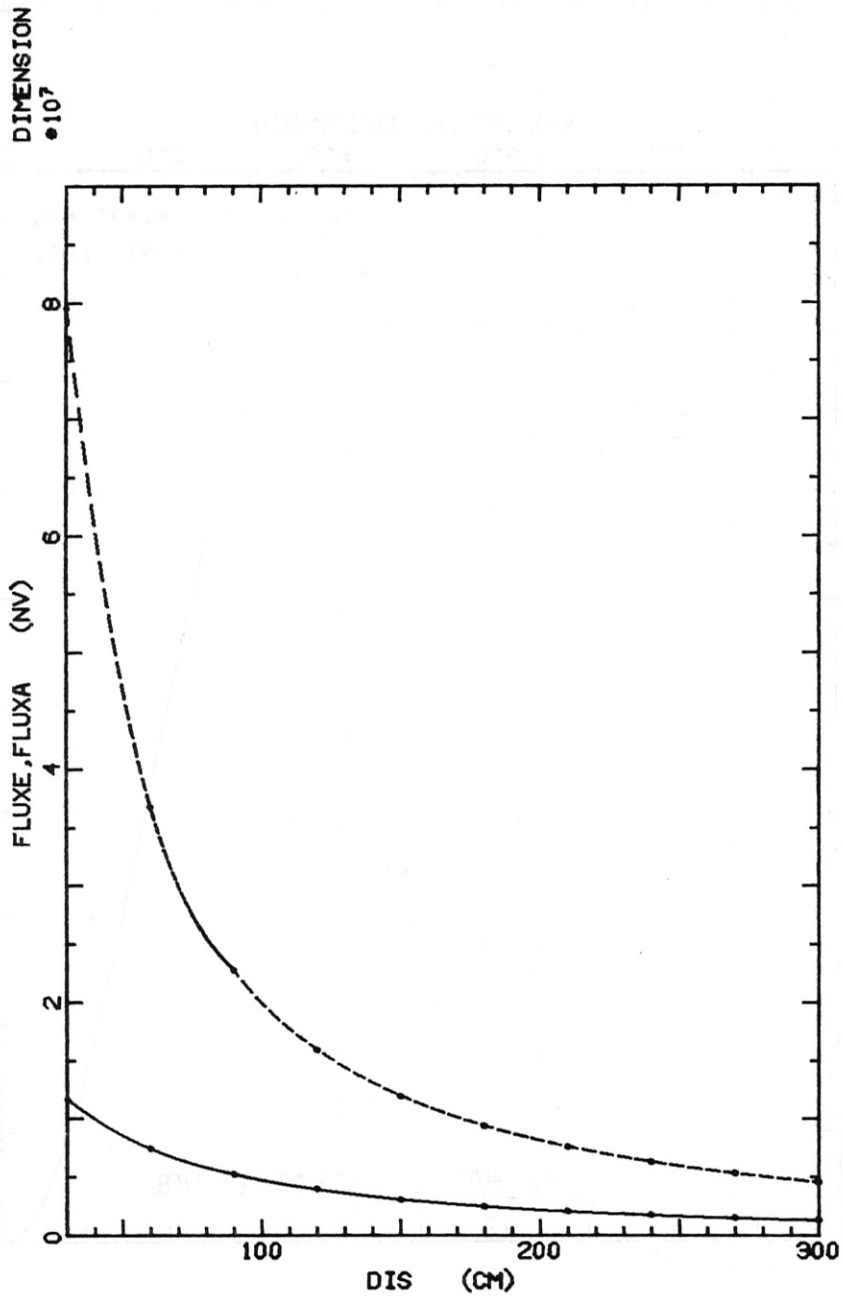

ASDEX TOKAMAK

CONTINUOUS LINE: EXACT SOLUTION FLUXE

DASHED LINE: APPROXIMATE SOLUTION FLUXA

TORUS MEAN RADIUS RT=164 (CM)

PLASMA RADIUS A=40 (CM)

HIGHEST ION DENSITY D0=1.E+14 (1/CCM)

HIGHEST ION TEMPERATURE T0=2 (KEV)

DENSITY PROFILE D=D0•(1-(R/A)••2)••2

TEMPERATURE PROFILE T=T0•(1-(R/A)••2)••2

REACTIVITY: SEE GAMOW EQUATION, D-D REACTIONS, N-BRANCH

Fig. 10 Exact and approximate calculation of the neutron flux in ASDEX tokamak

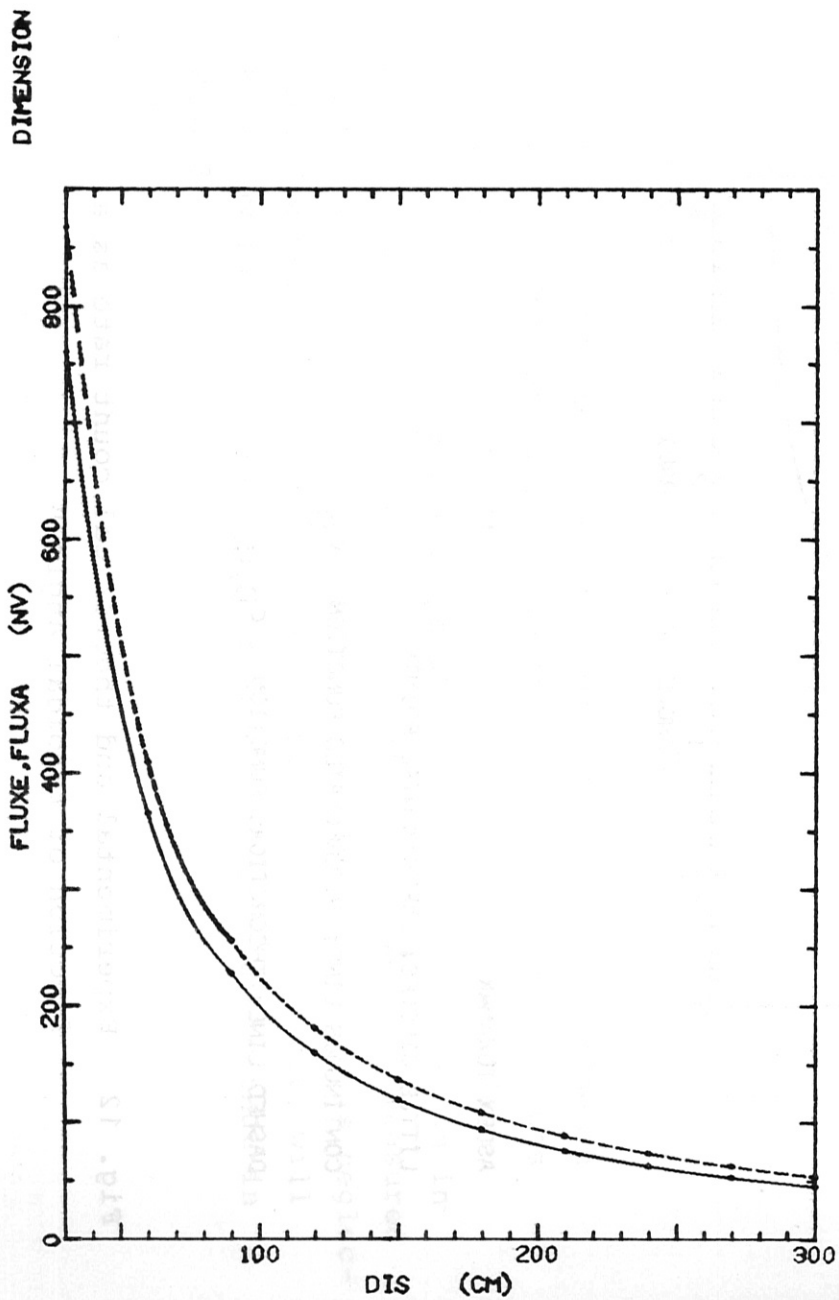

WENDELSTEIN VII STELLARATOR

CONTINUOUS LINE: EXACT SOLUTION FLUXE

DASHED LINE: APPROXIMATE SOLUTION FLUXA

TORUS MEAN RADIUS RT=200 (CM)

PLASMA RADIUS (FWHM) A=9 (CM)

HIGHEST ION DENSITY D0=7.2727E+13 (1/CCM)

HIGHEST ION TEMPERATURE T0=0.71 (KEV)

DENSITY PROFILE D=D0/(1+(R/A)**8)

TEMPERATURE PROFILE T=T0/(1+(R/A)**8)

REACTIVITY: SEE GAMOW EQUATION, D-D REACTIONS, N-BRANCH

Fig. 11 Exact and approximate calculation of the neutron flux in W VIIa stellarator

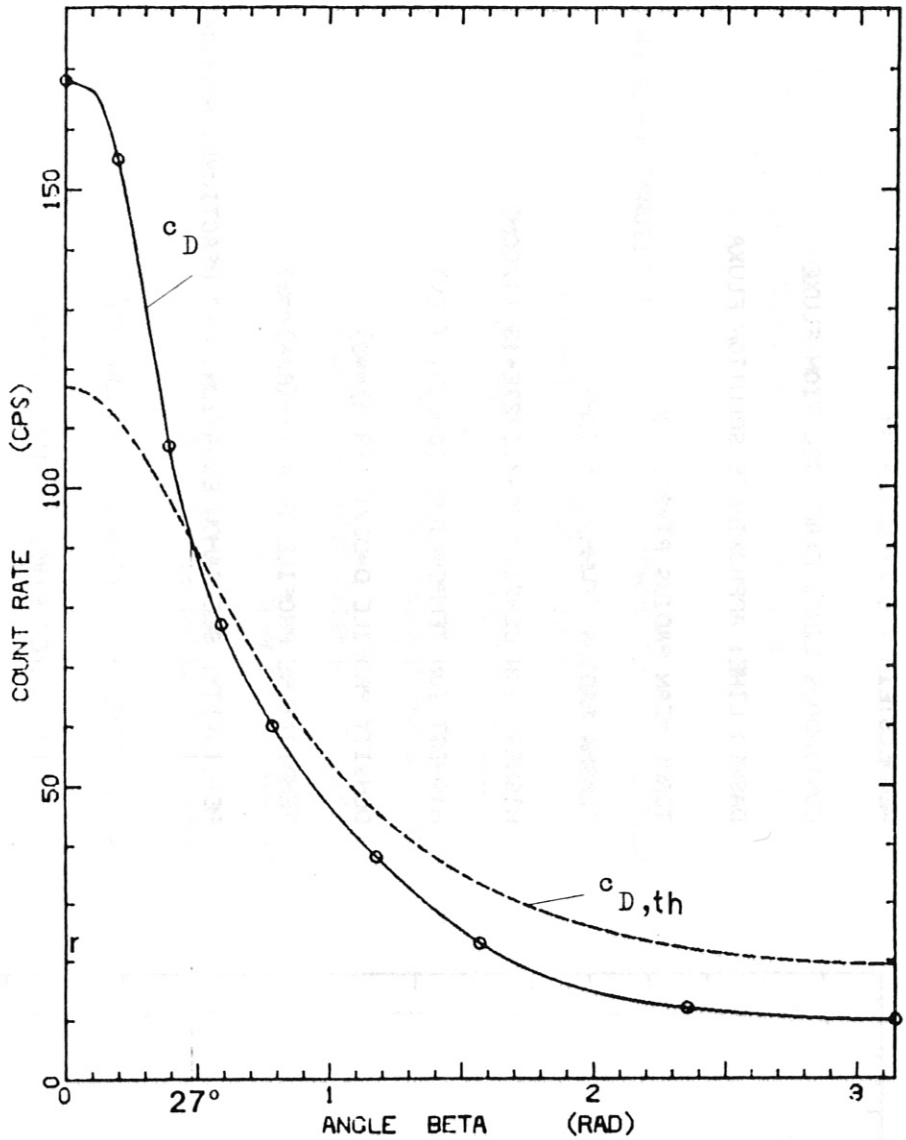

ASDEX TOKAMAK

LITTLE CIRCLES: EXPERIMENTAL POINTS

CONTINUOUS LINE: INTERPOLATED FUNCTION c_D

DASHED LINE: THEORETICAL FUNCTION $c_{D,th}$

Fig. 12 Experimental and theoretical count rate as a function of toroidal angle ß

detector (see Fig. 3). Only the last two points for bigger angles which could not be measured were obtained by extrapolation. The extrapolation was chosen in such a way that the condition

$$\int_0^{\P} C_{D,th}(\beta)\,d\beta = \int_0^{\P} C_D(\beta)\,d\beta$$

is satisfied.

Both count rate functions intersect in a point whose abscissa is $\beta = 27^{\circ}$. This result seems to be reasonable if one looks at Fig. 8: if the neutron source is placed at a positon with $\beta < 27^{\circ}$, the toroidal field coils increase the measured count rate as a consequence of neutron backscattering. By contrast, they act as a shield when $\beta > 27^{\circ}$. From the graph in Fig. 12 it is concluded that the deviation of the measured count rate from the calculated one in the case of a toroidal neutron source such as a plasma remains small as long as the viewing angle γ of the detecting system is matched to the space between two toroidal field coils (see Fig. 8).

4.2 Measurements at the W VIIa Stellarator

Figure 13 shows the ion density on the axis versus time in the W VIIa stellarator, as experimentally obtained. It was included in the input data of the C.TPROS computer code, which calculates the ion temperature. The result is shown in Figs. 14 and 15. Because the shielding effect was not measured in the stellarator, the function $S(\beta)$ (see eq. (24)) was neglected. The measurement error due to this effect, however, will keep low for all geometrical arrangements similar to that in Fig. 8.

a)

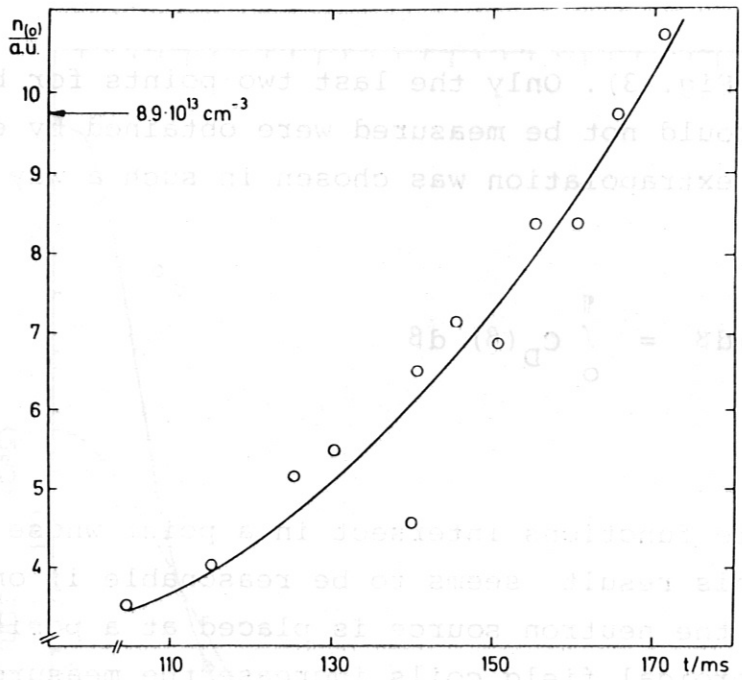

b)

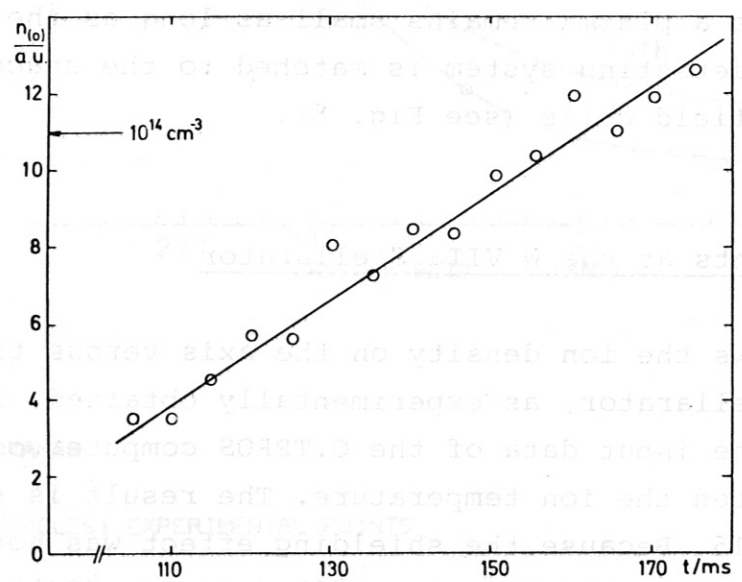

Fig. 13 Time evolution of ion density at the stellarator W VIIa
a): shots 21867 - 21882
b): shots 21966 - 21986

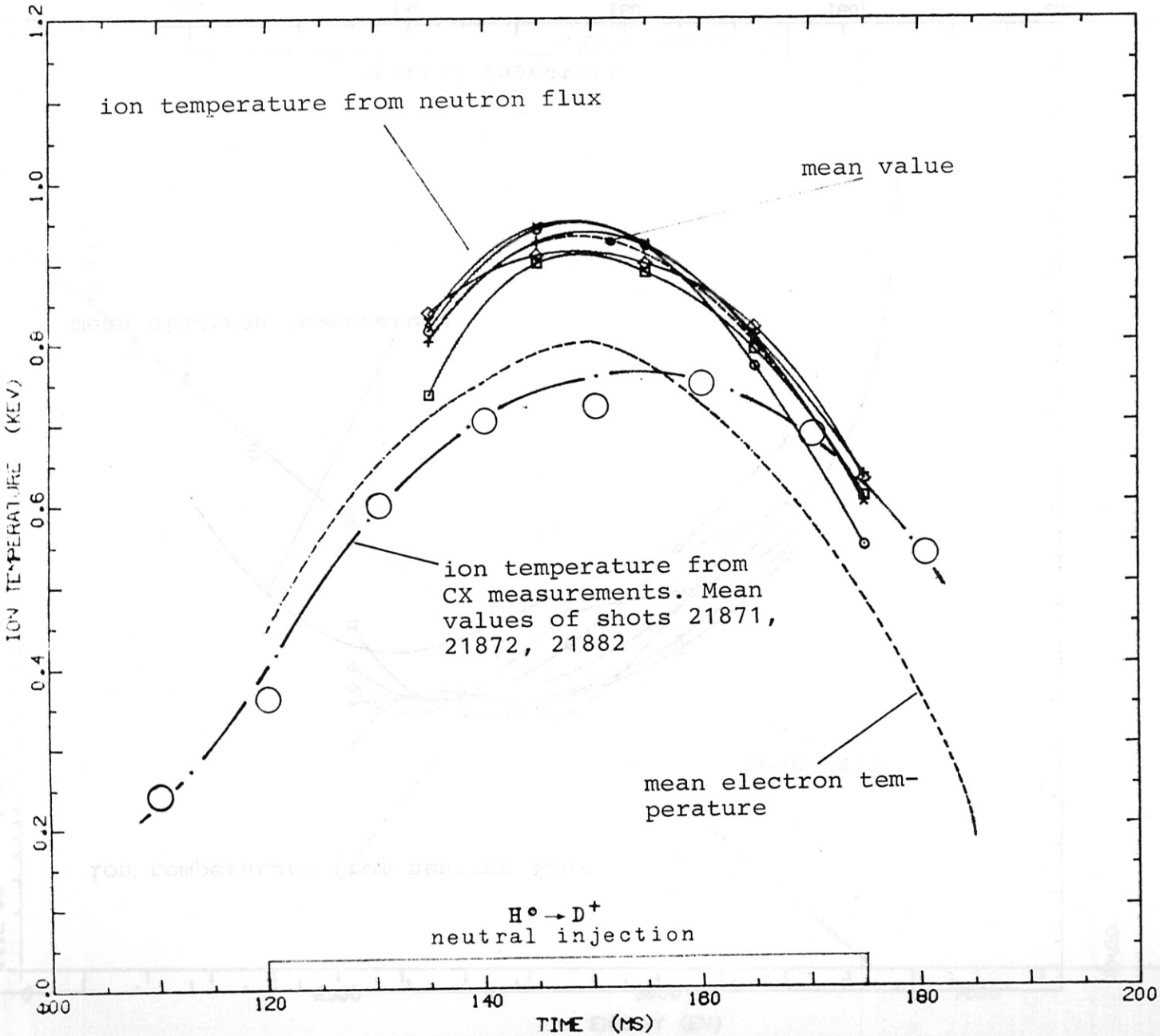

W VII A STELLARATOR

SHOTS 21871

21874

21875

21879

21882

Fig. 14 Time evolution of the temperature on the plasma axis. Density as in Fig. 13 a.

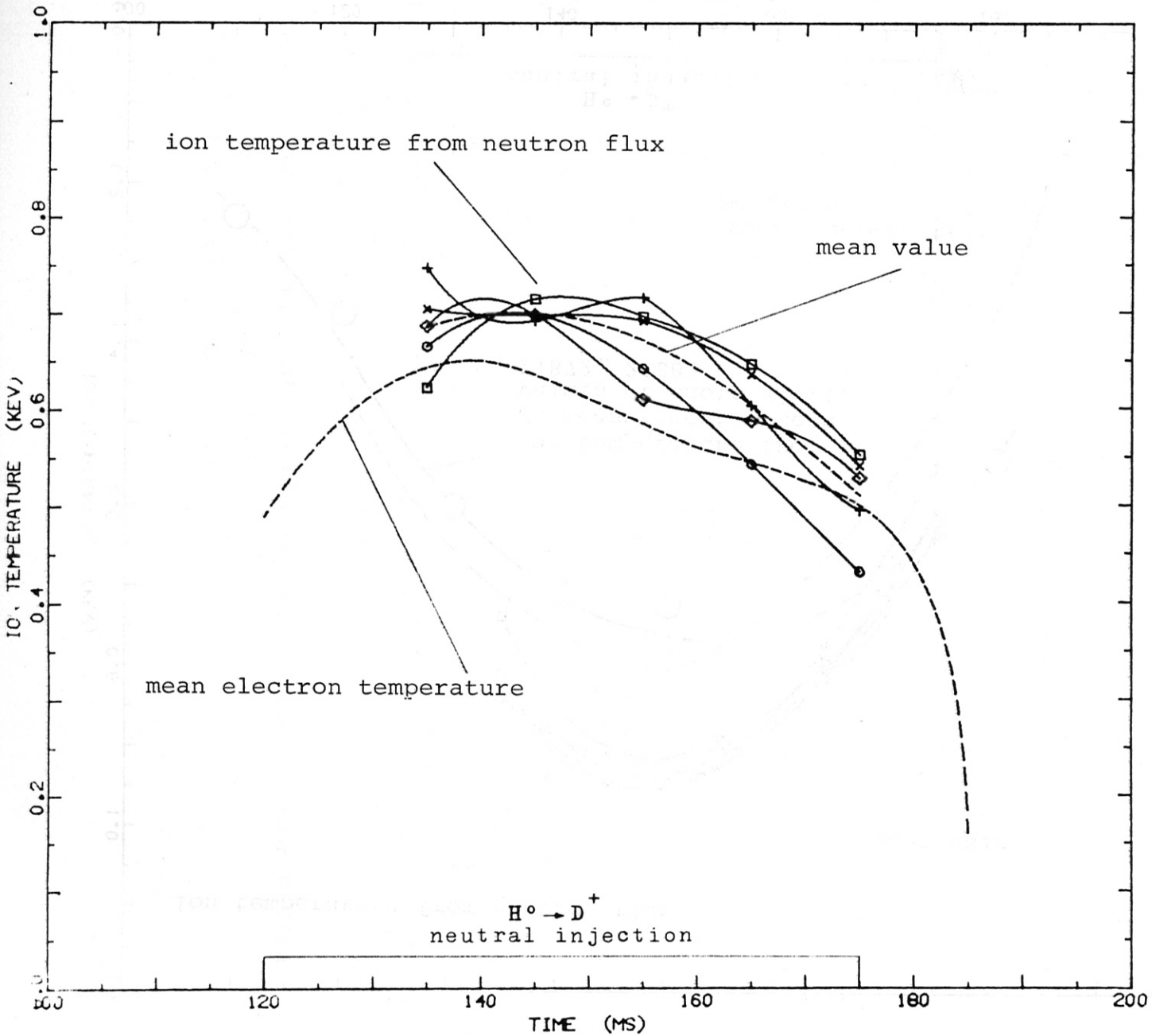

W VII A STELLARATOR

SHOTS 21970

21973

21975

21976

21978

Fig. 15 Time evolution of the ion temperature in W VIIa stellarator. Density as in Fig. 13 b.

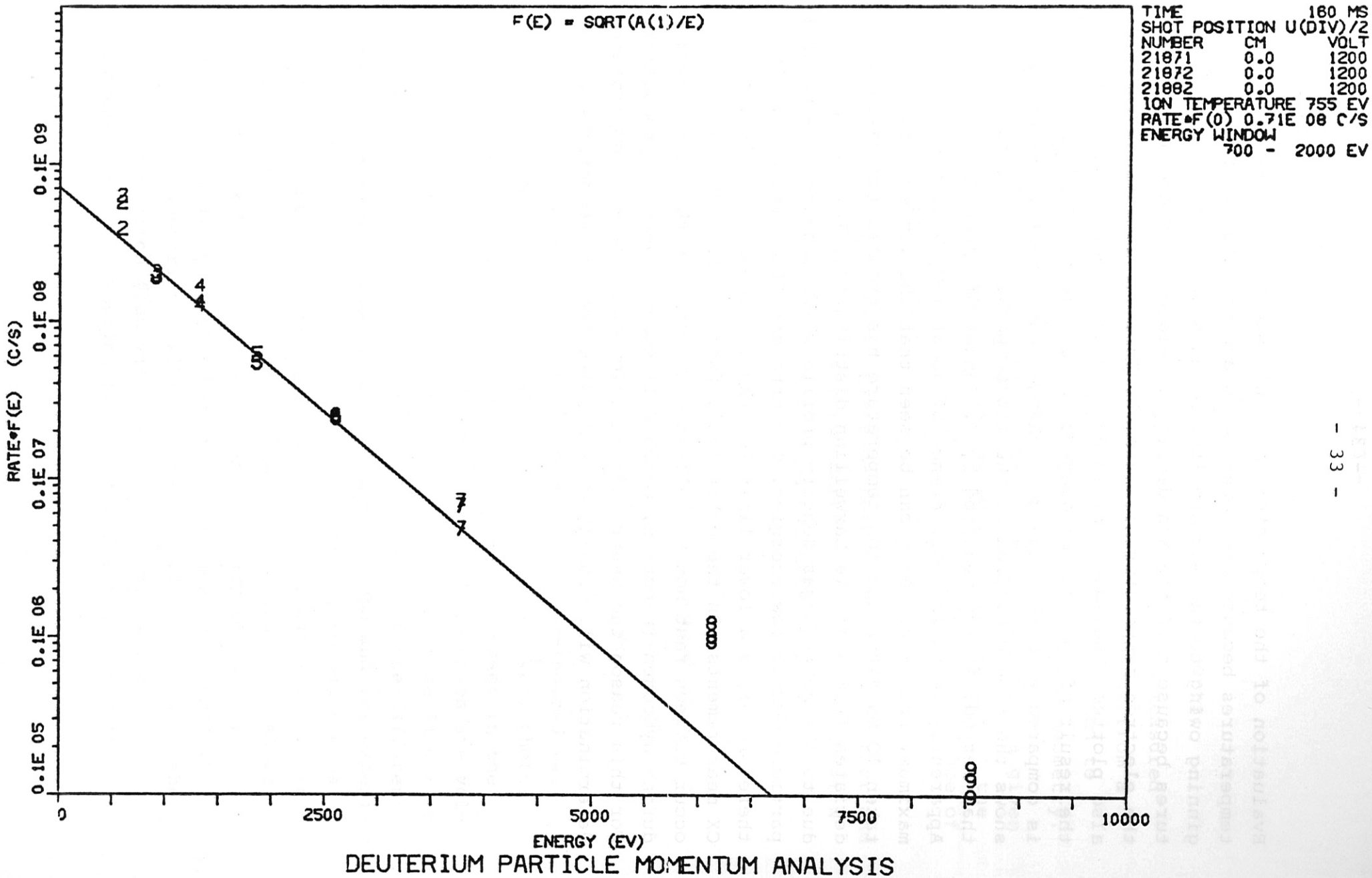

Fig. 16 Deuteron spectrum from CX measurements in W VIIa stellarator (by J. Junker).

Evaluation of the temperature can only start at higher temperatures because the count rates are too low at the beginning owing to the low density. It ends at lower temperatures because then the ion density is higher. For comparison, the electron temperature measured by Thompson scattering is also plotted. The agreement is quite good. A better check of the result of the neutron diagnostics can be obtained if it is compared with the charge exchange measurements. Figure 14 shows the time evolution of the ion temperature obtained by that method; it was measured by J. Junker of the W VIIa team. Apparently there is a difference of about 170 eV at the maximum. From Fig. 16 it can be seen that the ion spectrum taken 10 ms after the ion temperature has reached its maximum deviates from a simple Maxwellian distribution. This may be due to the neutral gas density profile which enhances the neutral particle flux at low energies. The straight line fit in Fig. 16 therefore gives a lower limit for the ion temperature from CX measurements. On the other hand, fusion reactions may occur between fast non Maxwellian deuterons and the bulk plasma during hydrogen injection, which will enhance neutron production. For this reason the neutron diagnostic method of ion temperature determination will usually overestimate the ion temperature.

5. Uncertainties, errors

The total error can be separated into two components:

- the error encurred in the neutron flux when the measured neutron flux is equated with the undisturbed flux from a toroidal thermonuclear plasma. This error is related to flux measurement including calibration and source geometry.
- the error in the ion temperature determination from a given neutron flux. This error is caused by uncertainties of the fusion reaction model, ion density and radial dependence of the ion temperature.

  The measuring error consists of both an accidental error and a systematic error. The first depends only on the number N of events which are counted in a counting period:

$$e_a = \frac{1}{\sqrt{N}} .$$

As has been explained in Sec. 2.1, the accidental error e_a is related to the neutron flux or count rate and to the time resolution required. It can easily be determined.

The systematic error is mainly caused by gamma-induced wall neutrons and by the calibration procedure. Moreover, photo-disintegration and electro-disintegration processes in the deuterium gas have to be considered. These processes are volume processes like fusion reactions. They cannot be discerned by thermal neutron detectors. The intensity of the different processes largely depends on the machine type and its experimental parameters. While it seems uncritical to use thermal neutron counters in stellarators, we expect difficulties in tokamaks if the gamma flux is high and the ion temperature is below 1 keV. In any case it is necessary to monitor the gamma flux. By means of hydrogen discharges and specially programmed deuterium discharges one should try to scale the parasitic neutron flux with the gamma flux. Geometrical asymmetry of the experiment, as given for tokamaks with

mechanical limiter, can also help to discern the different sources of the signal and reduce the error.

In ASDEX the investigations to solve this problem are under way. From comparison between hydrogen discharges and a few deuterium discharges at low ion temperatures and with high gamma flux we believe that deuterium disintegration processes do not play a significant role.

The error due to neutron flux calibration depends on the amount of scattered neutrons. If one uses a neutron fluxmeter which has been precisely calibrated elsewhere, one knows the actual flux Φ at the site of the detector:

$$\Phi = \frac{C}{\varepsilon},$$

where C is the measured count rate, and ε the given detector efficiency. The flux Φ can be regarded as composed of the undisturbed neutron flux Φ_1 from the voluminous toroidal plasma and the scattered flux Φ_s:

$$\Phi = \Phi_1 + \Phi_s.$$

The latter is not known. It is positive when the measured flux Φ is enhanced by backscattering, whereas it is negative when shielding is dominant. Its contribution represents the flux measurement error if one wishes to deduce the undisturbed flux Φ_1 from the measured flux Φ:

$$\Phi = \Phi_1 \left(1 + \frac{\Phi_s}{\Phi_1}\right). \qquad (30)$$

On the other hand, if one calibrates the detector at the site by means of a neutron source of known strength Q, one gets the count rate

$$C_c = \varepsilon \cdot \Phi_c = \varepsilon \cdot (\Phi_{1c} + \Phi_{sc}).$$

The index c indicates the calibration flux, and the index s the scattered component of the total flux Φ from the plasma or Φ_c from the calibration source.

The count rate C_c can be attributed to the undisturbed flux of the point-like calibration source in ideal field geometry by defining a suitable efficiency ε^*:

$$C_c = \varepsilon^* \cdot \Phi_{1c}.$$

Ideal means that the flux decreases as

$$\Phi_{1c} = \frac{Q}{4\pi D^2}, \qquad (31)$$

where D is the distance between the source and the detector. Consequently, the apparent counter efficiency ε^* determined by this method will be different from the true efficiency ε :

$$\varepsilon^* = \varepsilon\left(1 + \frac{\Phi_{sc}}{\Phi_{1c}}\right). \qquad (32)$$

By applying the apparent efficiency ε^* in the same way to determine the undisturbed flux Φ_1 from the plasma, one gets a measured quantity

$$\Phi^* = \frac{C}{\varepsilon^*} = \Phi_1 \left(1 + \frac{\Phi_s}{\Phi_1}(1-x)\right), \qquad (33)$$

with $x = \frac{\Phi_{sc}}{\Phi_c} \cdot \frac{\Phi}{\Phi_s}$.

In normal cases the range for x is

$$1 \geq x > 0.$$

From eq. (33) it can be recognized that the deviation of the measured flux Φ relative to the true primary flux Φ_1 is less than in eq. (30). The error becomes zero, i.e. $x = 1$, if the geometrical arrangements for calibration and measurement are equal. The error of the calibration method described by eq. (30) will only vanish if the scattered flux becomes zero. Different scattering caused by different neutron spectra would also contribute to the error. We believe this error to be very low because the spectrum of the ^{238}Pu-B neutron source is centred at 2.8 MeV and shows a steep decrease at the wings. There thus exists a similarity with the D-D neutron spectrum.

In ASDEX we have compared the two calibration methods. As long as neutron scattering or shielding is low the results will only slightly differ. Equation (31) is then quite well satisfied. Usually the detector is placed behind a thick lead shield. In this case calibration on site is superior and will be preferred. The remaining systematic error of the undisturbed neutron flux Φ_1 determined by means of eq. (33) is estimated to be not more than $\pm$10 %.

In fact, the geometries of the plasma and the calibration source are neither equal nor similar. We therefore measured the count rates when the calibration source was moved along the major radius of the torus (See also Sec. 3.3). Comparison of this measured function $C_D(\beta)$, where β is the toroidal angle, with the theoretical function $C_{D,th}(\beta)$, yields a correcting function $S(\beta)$. Neglecting $S(\beta)$ results in a change of -3 % for the ion temperature, which corresponds to a flux error of -14 % at 2 keV (Fig. 17). The overall systematic error of the undisturbed neutron flux from the plasma, neglecting gamma-induced

neutron production, can therefore be assumed not to exceed ±24 %.

The calculation of the ion temperature of the plasma from the neutron flux calls for some assumptions. The basic one is the fusion reaction model. For several reasons ASDEX will be operated preferably with deuterium plasma and heated by a hydrogen beam. This operation mode allows the assumption of a Maxwellian ion distribution (Ref. 11). With a deuterium beam, fusion reactions between the beam ions and the bulk plasma play a dominant role, and interpretation of the neutron measurements becomes difficult.

The measured neutron flux represents an integral value which includes the ion density and the ion temperature as functions of the radius. It is obvious that the normalized profiles and the absolute ion density must be known to calculate the ion temperature on the axis. Without considering the neutron flux error the error for the ion temperature is therefore composed of two additional sources of error:

- error of the ion density
- error due to the assumption on the normalized radial temperature profile.

The ion density profile is derived from the electron density profile taking into account the impurities by means of Z_{eff}. At ASDEX Z_{eff} usually is 1. For $Z_{eff} < 1.5$ the difference between electron density and ion density is small.

The temperature error relative to the error of the experimentally determined neutron flux of the plasma can be derived from the Gamov equation and is given in Fig. 17. In the temperature region of a few keV this ratio is low. This means the neutron flux measurement at moderate temperatures gives a rather accurate temperature value. With an error of about 15 % for the neutron flux one gets an error of 3.3 % for the ion temperature at $T_i = 2$ keV. This becomes worse for higher temperatures.

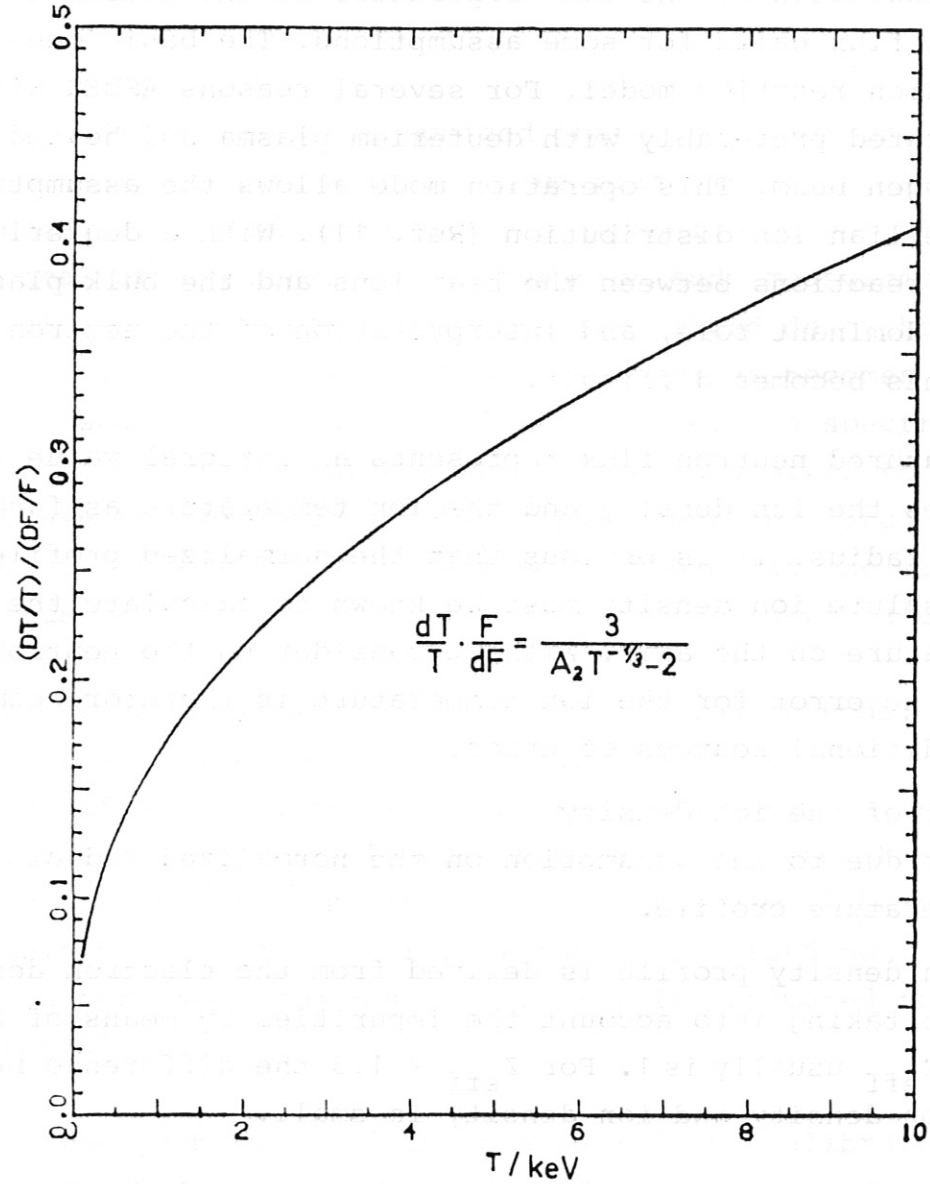

Fig. 17 Ratio of ion temperature error and neutron flux error.

The temperature error due to the error of the maximum ion density is always less than the latter at temperatures of a few keV because the reaction rate depends much more on the ion temperature than on the density (see eq. 3 and Fig. 6). The sensitivity of the calculated temperature to the assumed profiles was numerically determined. For the calculation of the overall systematic error of the ion temperature in Table 1 it was assumed that the different factors are statistically independent.

source of error	Uncertainty, error/%	Corresponding temperature error/%
Neutron flux measurement	+24/-24	+5/-5
Density	+10/-10	-3/+3
Radial Profiles, FWHM	+23/-16	-13/+6
Total temperature error		+8/-14 %

Table 1. Estimated range of systematic errors neglecting non-thermonuclear fusion reactions.

From the arguments and figures given above we draw the conclusion that the accuracy of the ion temperature determination by means of neutron flux measurement is satisfactory if the ion temperature is in the range of 1 keV to 3 keV. This range corresponds to the ASDEX experimental regime. The test measurements in the W VIIa stellarator confirmed this statement. Factors which affect the accuracy of the flux signal have little influence on the temperature accuracy. Input data such as density and profile functions are more important. The dominant factors are the fusion reaction kinetics and the gamma-induced neutron production. They depend on the fusion machine and its experimental parameters. If non-thermonuclear and

gamma-induced reactions cause considerable neutron flux, the error for the ion temperature evaluation cannot be estimated.

Acknowledgement

The authors wish to thank P. Smeulders, A. Weller and J. Junker of the stellarator team for their assistance with the test measurements.

6. Appendices

Appendix 1

Some details about the numerical evaluation of integrals (10) and (15) are briefly considered here. A very simple method to solve the integral of a continuous not oscillating function f(x) with its derivatives is the Gaussian quadrature:

$$\int_a^b f(x)dx = \frac{b-a}{2} \int_{-1}^{+1} f\left(\frac{b-a}{2} \cdot t + \frac{b+a}{2}\right)dt \qquad (A1\text{-}1)$$

$$= \frac{b-a}{2} \lim_{N \to \infty} \sum_1^N{}_i \; f\left(\frac{b-a}{2} P_i + \frac{b+a}{2}\right) W_i,$$

where the integration range [a,b] is limited, and P_i, W_i are the Gaussian nodes and weights. The reduction of the interval [a,b] into the standard one [-1,1] is necessary because the set of points P_i is defined on this standard range. The generalization of eq. (A1-1) for a multiple integral is evident, e.g. for a double integral

$$\int_a^b dx \int_c^d f(x,y)\, dy = \frac{(b-a)\;(d-c)}{4} \; . \qquad (A1\text{-}2)$$

$$\cdot \lim_{M,N \to \infty} \sum_1^M{}_i \sum_1^N{}_j f\left(\frac{b-a}{2} P_i + \frac{b+a}{2}, \frac{d-c}{2} P_j + \frac{d+c}{2}\right) W_i W_j .$$

Such formulas can very easily be handled by a computer: a DO cycle performs each summation, while a FUNCTION subprogram computes the value of the function in the correct point. The only disadvantage is that the integrand must be evaluated in a large set of points, if the number of nodes required for good convergence is high and the integral is multiple; as a consequence the computing time may become excessive. The C. FLUXED and C. FLUXAD computer codes perform the integrations of eq. (10) and (15). The meanings of the symbols and of some parts of the codes are explained by comment cards.

Appendix 2

The zero point of the function (22), i.e. the solution of equation

$$F(T_{o,i}) = 0 \qquad \text{(A2-1)}$$

for each i, is found by an iterative method that uses a given interval, that is assumed to contain the zero. The approximate root is accepted as the real root when the corresponding value of the function is less than a fixed error (first convergence criterion), or when the results of two successive iterations agree to a given number of significant digits (second convergence criterion). The C. TPROS computer code is used to find the solution of eq. (A2-1) for each value of i, the shielding effect (see Sec. 3.3) being taken into account. The results thus obtained, must then be plotted versus time to have ion temperature as a function of time.

Appendix 3

The functions $C_{D,th}(\beta)$, $C_D(\beta)$ and $S(\beta)$ defined by eq. (24) are computed by means of the B. FIT code. The function $C_{D,th}(\beta)$ is analytically evaluated in the set of points $\{\pi P_i\}$, i = 1,...,N, where $\{P_i\}$ are the Gaussian nodes (see Appendix 1). The reason for this choice is that the values $C_{D,th}(\pi P_i)$ are needed if the integrals eq. (27) or eq. (29) have to be solved by the Gaussian quadrature method.

The function $C_D(\beta)$ is experimentally known in a set of points $\{\beta_i\}$, i = 1,...,17. It is therefore interpolated in $\{\pi P_i\}$ i = 1,...,N for the same reason. Finally, the values $S(\pi P_i)$ are computed. The interpolation is made by a cubic spline with second derivatives. It is assumed that

$$C_D''(0) = C_D''(\pi) = 0 \qquad \text{(A3-1)}$$

The B. FIT code also gives the plot of the functions $C_{D,th}(\beta)$ and $C_D(\beta)$ versus the angle .

```
C  C.FLUXED
C  DOUBLE PRECISION PROGRAM
C  DATA ARE IN A.DATA
C  THIS PROGRAM GIVES AN EXACT SOLUTION FOR THE NEUTRON FLUX
C  GENERATED BY A TOROIDAL VOLUME OF PLASMA: IT IS VALID FOR VARIOUS
C  DISTANCES FROM THE TORUS.
C  THE SYMBOLS USED ARE:
C  R  RADIUS (CM)
C  A  PLASMA RADIUS (CM)
C  RT  TORUS MEAN RADIUS (CM)
C  D  ION DENSITY AS A FUNCTION OF R (1/CC)
C  D0  ION DENSITY FOR R=0 (1/CC)
C  T  ION TEMPERATURE AS A FUNCTION OF R (KEV)
C  T0  ION TEMPERATURE FOR R=0 (KEV)
C  B1,B2,B3,B4  EXPONENTS IN ION DENSITY AND ION TEMPERATURE PROFILES
C  A1,A2  COEFFICIENTS IN GAMOW EQUATION
C  RDD  REACTIVITY FOR D-D REACTIONS, NEUTRON BRANCH (1/CC SEC)
C  P10(10),...,P60(60)  GAUSSIAN POINTS
C  W10(10),...,W60(60)  GAUSSIAN WEIGTHS
C  PN  NEUTRONS PRODUCED PER SEC BY THE PLASMA TORUS (1/SEC)
C  FLUX  NEUTRON FLUX GENERATED BY THE PLASMA TORUS (NV)
C  ALFA,BETA  ANGLES (RADIANS)
C  GP  GREEK PI
C  DIST,BE,DE  DISTANCES (CM)
C  SB2,DS2  SQUARE DISTANCE (SQCM)
C  DIS  DISTANCE BETWEEN THE POINT IN WHICH THE FLUX IS COMPUTED AND THE
C  SURFACE OF THE TORUS (CM)
C  N  NUMBER OF USED GAUSSIAN POINTS
C
      IMPLICIT REAL*8(A-H,O-Z)
      DIMENSION P10(10),P20(20),P30(30),P40(40),P50(50),P60(60)
      DIMENSION W10(10),W20(20),W30(30),W40(40),W50(50),W60(60)
      INTEGER B1,B2,B3,B4
      COMMON/FIT/DIS,RT,GP
      COMMON/FIZ/B1,B2,B3,B4,A1,A2
      COMMON/FIL/D0,T0,A
      COMMON/FIW/AL
C  READING AND WRITING OF GAUSSIAN POINTS AND WEIGTHS
      READ(5,4)P10,W10
      READ(5,4)P20,W20
      READ(5,4)P30,W30
      READ(5,4)P40,W40
      READ(5,4)P50,W50
      READ(5,4)P60,W60
    4 FORMAT(5D12.5)
      WRITE(6,1)
    1 FORMAT(11X,'P10',19X,'W10',19X,'P20',19X,'W20',19X,'P30',19X,'W30'
     */)
      DO 3 I=1,10
      WRITE(6,5)P10(I),W10(I),P20(I),W20(I),P30(I),W30(I)
    3 CONTINUE
      DO 7 I=11,20
      WRITE(6,9)P20(I),W20(I),P30(I),W30(I)
    7 CONTINUE
      DO 11 I=21,30
      WRITE(6,13)P30(I),W30(I)
   11 CONTINUE
```

```
5800          WRITE(6,15)
5900       15 FORMAT(////11X,'P40',19X,'W40',19X,'P50',19X,'W50',19X,'P60',19X,'
6000         *W60'/)
6100          DO 17 I=1,40
6200          WRITE(6,5)P40(I),W40(I),P50(I),W50(I),P60(I),W60(I)
6300       17 CONTINUE
6400          DO 19 I=41,50
6500          WRITE(6,9)P50(I),W50(I),P60(I),W60(I)
6600       19 CONTINUE
6700          DO 21 I=51,60
6800          WRITE(6,13)P60(I),W60(I)
6900       21 CONTINUE
7000        5 FORMAT(1X,6(D17.10,5X))
7100        9 FORMAT(45X,4(D17.10,5X))
7200       13 FORMAT(89X,2(D17.10,5X))
7300 C     DATA FOR ASDEX TOKAMAK:
7400          A=40.D0
7500          RT=164.D0
7600          DIST=30.D0
7700          D0=3.D+13
7800          T0=1.D0
7900          B1=2
8000          B2=2
8100          B3=2
8200          B4=2
8300 C     DATA FOR WENDELSTEIN VII STELLARATOR:
8400 C        A=3.D0
8500 C        RT=200.D0
8600 C        DIST=30.D0
8700 C        D0=7.27273D+13
8800 C        T0=0.71D0
8900 C        B1=3
9000 C        B2=3
9100 C     REACTIVITY PARAMETERS (GAMOW EQUATION)
9200          A1=3.4920841D-14
9300          A2=20.144728D0
9400 C     GREEK PI AND NUMBER OF USED GAUSSIAN NODES
9500          GP=3.1415926D0
9600          N=60
9700 C     COMPUTATION OF THE INTEGRAL GIVING FLUX AND RESULT'S PRINTING
9800 C     THE FLUX IS COMPUTED FOR VARIOUS DISTANCES DIS
9900          DO 10 I=1,10
10000         DIS=DIST*I
10100 C     AU IS THE UPPER LIMIT OF THE SPACE INTEGRAL. FOR ASDEX IT IS AU=A,
10200 C     FOR W VII IT IS AU=10.D0
10300         AU=A
10400         FLUX=0.D0
10500         DO 20 J=1,60
10600         DO 30 K=1,60
10700         DO 40 L=1,60
10800         FLUX=FLUX+FCT(P60(J),P60(K),P60(L))*W60(J)*W60(K)*W60(L)
10900      40 CONTINUE
11000      30 CONTINUE
11100      20 CONTINUE
11200         FLUX=FLUX*(AU/2.D0)*GP*GP
11300         WRITE(6,50)N,DIS,FLUX
11400      50 FORMAT(10X,'N=',I2,10X,'DIS=',F4.0,'  (CM)',10X,'FLUX=',D17.10,'
```

```
11500       *(NV)')
11600    10  CONTINUE
11700       STOP
11800       END
11900 C
12000 C
12100       FUNCTION FCT(R,ALFA,BETA)
12200       IMPLICIT REAL*8(A-H,O-Z)
12300       INTEGER B1,B2,B3,B4
12400       COMMON/FIT/DIS,RT,GP
12500       COMMON/FIZ/B1,B2,B3,B4,A1,A2
12600       COMMON/FIL/DO,TO,A
12700       COMMON/FIW/AL
12800       RX=(AL/2.D0)*(R+1.D0)
12900       ALFAY=GP*(ALFA+1.D0)
13000       BETAZ=GP*BETA
13100 C  VOL IS THE VOLUME ELEMENT
13200       VOL=RX*(RT-RX*DCOS(ALFAY))
13300 C  DENSITY AND TEMPERATURE SPACE PROFILES FOR ASDEX
13400       D=DO*(1.D0-(RX/A)**B1)**B2
13500       T=TO*(1.D0-(RX/A)**B3)**B4
13600 C  DENSITY AND TEMPERATURE SPACE PROFILES FOR W VII
13700 C     D=DO/(1.D0+(RX/A)**B1)
13800 C     T=TO/(1.D0+(RX/A)**B2)
13900 C  RDD IS THE REACTION RATE, ACCORDING TO GAMOW EQUATION, FOR D-D
14000 C  REACTIONS, NEUTRON BRANCH
14100       RDD=(0.5D0*D**2)*(A1*T**(-2.D0/3.D0)*DEXP(-A2*T**(-1.D0/3.D0)))
14200 C  GEOMETRIC RELATIONS
14300       SB2=(RX*DSIN(ALFAY))**2+((RT-RX*DCOS(ALFAY))*DTAN(BETAZ))**2
14400       BE=DABS(DSQRT(SB2))*DABS(DSIN(BETAZ))
14500       DE=RT+A*DIS+BE-(RT-RX*DCOS(ALFAY))/DCOS(BETAZ)
14600       DS2=SB2*(DCOS(BETAZ)**2)+DE**2
14700 C  FCT IS THE INTEGRAND FUNCTION
14800       FCT=VOL*RDD/(4.D0*GP*DS2)
14900       RETURN
15000       END
```

```
C  C.FLUXAD
C  DOUBLE PRECISION PROGRAM
C   DATA ARE IN A1.DATA
C  THIS PROGRAM GIVES AN APPROXIMATE SOLUTION FOR THE NEUTRON FLUX
C  GENERATED BY A TOROIDAL VOLUME OF PLASMA: IT IS VALID FOR LARGE
C  DISTANCES FROM THE TORUS.
C  THE SYMBOLS USED ARE:
C  R  RADIUS (CM)
C  A  PLASMA RADIUS (CM)
C  RT  TORUS MEAN RADIUS (CM)
C  D  ION DENSITY AS A FUNCTION OF R (1/CC)
C  D0  ION DENSITY FOR R=0 (1/CC)
C  T  ION TEMPERATURE AS A FUNCTION OF R (KEV)
C  T0  ION TEMPERATURE FOR R=0 (KEV)
C  B1,B2,B3,B4  EXPONENTS IN ION DENSITY AND ION TEMPERATURE PROFILES
C  A1,A2  COEFFICIENTS IN GAMMA EQUATION
C  RDD  REACTIVITY FOR D-D REACTIONS, NEUTRON BRANCH (1/CC SEC)
C  P10(10),...,P60(60)  GAUSSIAN POINTS
C  W10(10),...,W60(60)  GAUSSIAN WEIGTHS
C  PN  NEUTRONS PRODUCED PER SEC BY THE PLASMA TORUS (1/SEC)
C  FLUX  NEUTRON FLUX GENERATED BY THE PLASMA TORUS (NV)
C  ALFA,BETA  ANGLES (RADIANS)
C  GP  GREEK P
C  DS2  SQUARE DISTANCE (SQCM)
C  DIS  DISTANCE BETWEEN THE POINT IN WHICH THE FLUX IS COMPUTED AND THE
C    SURFACE OF THE TORUS (CM)
C  DIST  DISTANCE (CM)
C  N  NUMBER OF USED GAUSSIAN POINTS
C
      IMPLICIT REAL*8(A-H,O-Z)
      DIMENSION P10(10),P20(20),P30(30),P40(40),P50(50),P60(60)
      DIMENSION W10(10),W20(20),W30(30),W40(40),W50(50),W60(60)
      INTEGER B1,B2,B3,B4
      COMMON/FIT/DIS,RT,GP
      COMMON/FIZ/B1,B2,B3,B4,A1,A2
      COMMON/FIL/D0,T0,A
      COMMON/FIC/PN
      COMMON/FIW/AL
C  READING AND WRITING OF GAUSSIAN POINTS AND WEIGTHS
      READ(5,4)P10,W10
      READ(5,4)P20,W20
      READ(5,4)P30,W30
      READ(5,4)P40,W40
      READ(5,4)P50,W50
      READ(5,4)P60,W60
    4 FORMAT(5D12.5)
      WRITE(6,1)
    1 FORMAT(11X,'P10',19X,'W10',19X,'P20',19X,'W20',19X,'P30',19X,'W30'
     */)
      DO 3 I=1,10
      WRITE(6,5)P10(I),W10(I),P20(I),W20(I),P30(I),W30(I)
    3 CONTINUE
      DO 7 I=11,20
      WRITE(6,9)P20(I),W20(I),P30(I),W30(I)
    7 CONTINUE
      DO 11 I=21,30
      WRITE(6,13)P30(I),W30(I)
```

```
      11  CONTINUE
          WRITE(6,15)
      15  FORMAT(////11X,'P40',19X,'W40',19X,'P50',19X,'W50',19X,'P60',19X,'
     *W60'/)
          DO 17 I=1,40
          WRITE(6,5)P40(I),W40(I),P50(I),W50(I),P60(I),W60(I)
      17  CONTINUE
          DO 19 I=41,50
          WRITE(6,9)P50(I),W50(I),P60(I),W60(I)
      19  CONTINUE
          DO 21 I=51,60
          WRITE(6,13)P60(I),W60(I)
      21  CONTINUE
       5  FORMAT(1X,6(D17.10,5X))
       9  FORMAT(45X,4(D17.10,5X))
      13  FORMAT(89X,2(D17.10,5X))
C     DATA FOR ASDEX TOKAMAK:
          A=40.D0
          RT=164.D0
          DIST=30.D0
          D0=3.D+13
          T0=2.D0
          B1=2
          B2=2
          B3=2
          B4=2
C     DATA FOR WENDELSTEIN VII STELLARATOR
C         A=3.D0
C         RT=200.D0
C         DIST=30.D0
C         D0=7.27273D+13
C         T0=0.7100
C         B1=3
C         B2=3
C      REACTIVITY PARAMETERS (GAMOW EQUATION)
          A1=3.4920841D-14
          A2=20.144728D0
C     GREEK PI AND NUMBER OF USED GAUSSIAN NODES
          GP=3.1415926D0
          N=60
C     COMPUTATION OF THE INTEGRAL GIVING PN AND RESULT'S PRINTING
C     AU IS THE UPPER LIMIT OF THE SPACE INTEGRAL. FOR ASDEX IT IS AU=A,
C     FOR W VII IT IS AU=10.D0
          AU=A
          PN=0.D0
          DO 10 I=1,60
          DO 20 J=1,60
          PN=PN+FCT(P60(I),P60(J))*W60(I)*W60(J)
      20  CONTINUE
      10  CONTINUE
          PN=PN*(AU/2.D0)*GP
          WRITE(6,25)N
      25  FORMAT(////30X,'N=',I2//)
          WRITE(6,30)PN
      30  FORMAT(30X,'PN=',D15.8,'  (1/SEC)'//)
C     COMPUTATION OF INTEGRAL GIVING FLUX AND RESULT'S PRINTING. THE
C     FLUX IS COMPUTED FOR VARIOUS DISTANCES DIS
```

```
11500       DO 50 I=1,10
11600       DIS=DIST*I
11700       FLUX=0.D0
11800       DO 35 K=1,60
11900       FLUX=FLUX+FFCT(P60(K))*W60(K)
12000    35 CONTINUE
12100       FLUX=FLUX*GP
12200       WRITE(6,40)DIS,FLUX
12300    40 FORMAT(30X,'DIS=',F4.0,'  (CM)',15X,'FLUX=',D15.8,'  (NV)'//)
12400    50 CONTINUE
12500       STOP
12600       END
12700 C
12800 C
12900       FUNCTION FCT(R,ALFA)
13000       IMPLICIT REAL*8(A-H,O-Z)
13100       INTEGER B1,B2,B3,B4
13200       COMMON/FIT/DIS,RT,GP
13300       COMMON/FIZ/B1,B2,B3,B4,A1,A2
13400       COMMON/FIL/DO,TO,A
13500       COMMON/FIW/AL
13600       RX=(AL/2.D0)*(R+1.D0)
13700       ALFAY=GP*(ALFA+1.D0)
13800 C   VOL IS THE VOLUME ELEMENT
13900       VOL=RX*(RT-RX*DCOS(ALFAY))
14000 C   DENSITY AND TEMPERATURE SPACE PROFILES FOR ASDEX
14100 C      D=DO*(1.D0-(RX/A)**B1)**B2
14200 C      T=TO*(1.D0-(RX/A)**B3)**B4
14300 C   DENSITY AND TEMPERATURE SPACE PROFILES FOR W VII
14400       D=DO/(1.D0+(RX/A)**B1)
14500       T=TO/(1.DO+(RX/A)**B2)
14600 C   RDD IS THE REACTION RATE, ACCORDING TO GAMOW EQUATION, FOR D-D
14700 C   REACTIONS, NEUTRON BRANCH
14800       RDD=(0.5DO*D**2)*(A1*T**(-2.D0/3.D0)*DEXP(-A2*T**(-1.DO/3.DO)))
14900 C   FCT IS THE INTEGRAND FUNCTION TO COMPUTE PN
15000       FCT=2.D0*GP*VOL*RDD
15100       RETURN
15200       END
15300 C
15400 C
15500       FUNCTION FFCT(BETA)
15600       IMPLICIT REAL*8(A-H,O-Z)
15700       COMMON/FIT/DIS,RT,GP
15800       COMMON/FIC/PN
15900       BETAX=BETA*GP
16000       DS2=(DIS+RT)**2+RT**2-2.D0*(DIS+RT)*RT*DCOS(BETAX)
16100 C   FFCT IS THE INTEGRAND FUNCTION TO COMPUTE THE FLUX
16200       FFCT=PN/(8.D0*GP**2*DS2)
16300       RETURN
16400       END
```

```
C    C.TPRCS
C    DATA ARE IN A1.DATA, A1.DATAF, A1.SHOT
C    A1.DATA CONTAINS THE GAUSSIAN POINTS AND WEIGHTS
C    A1.DATAF CONTAINS THE EXP. COUNT RATES TO FIT THE SHIELDING
C    FUNCTION
C    A1.SHOT CONTAINS THE DATA REFERRING TO A CERTAIN SHOT
C    THIS PROGRAM COMPUTES THE TIME DEPENDENCE OF THE ION TEMPERATURE,
C    TAKING INTO ACCOUNT THE SHIELDING EFFECT
C    THE USED UNITS ARE: CM FOR SPACE, SEC FOR TIME, KEV FOR TEMPERATURE,
C    CPS/NV FOR THE EFFICIENCY OF THE DETECTING SYSTEM
      IMPLICIT REAL*8(A-H,O-Z)
      DIMENSION P10(10),P20(20),P30(30),P40(40),P50(50),P60(60)
      DIMENSION W10(10),W20(20),W30(30),W40(40),W50(50),W60(60)
      DIMENSION TIME(5),FM(5),DO(5)
      DIMENSION X(9),Y(9),BPAR(4),C(9,3)
      DIMENSION UU(30),U(30),S(30),SS(60)
      INTEGER B1,B2,B3,B4
      INTEGER NX,IC,M,IER
      COMMON/NOD/P10,P20,P30,P40,P50,P60
      COMMON/WEI/W10,W20,W30,W40,W50,W60
      COMMON/FIT/DIS,RT,GP
      COMMON/FIZ/B1,B2,B3,B4,A1,A2
      COMMON/FIL/DO,A,IND
      COMMON/FIW/FM,CHT,EFF,C
      COMMON/SHI/SS
      COMMON/COR/COEF
      EXTERNAL FLUX
C  READING AND WRITING OF GAUSSIAN POINTS AND WEIGTHS
      READ(5,4)P10,W10
      READ(5,4)P20,W20
      READ(5,4)P30,W30
      READ(5,4)P40,W40
      READ(5,4)P50,W50
      READ(5,4)P60,W60
    4 FORMAT(5D12.5)
      WRITE(6,1)
    1 FORMAT(11X,'P10',19X,'W10',19X,'P20',19X,'W20',19X,'P30',19X,'W30'
     *//)
      DO 3 I=1,10
      WRITE(6,5)P10(I),W10(I),P20(I),W20(I),P30(I),W30(I)
    3 CONTINUE
      DO 7 I=11,20
      WRITE(6,9)P20(I),W20(I),P30(I),W30(I)
    7 CONTINUE
      DO 11 I=21,30
      WRITE(6,13)P30(I),W30(I)
   11 CONTINUE
      WRITE(6,15)
   15 FORMAT(////11X,'P40',19X,'W40',19X,'P50',19X,'W50',19X,'P60',19X,'
     *W60'//)
      DO 17 I=1,40
      WRITE(6,5)P40(I),W40(I),P50(I),W50(I),P60(I),W60(I)
   17 CONTINUE
      DO 19 I=41,50
      WRITE(6,9)P50(I),W50(I),P60(I),W60(I)
   19 CONTINUE
      DO 21 I=51,60
```

```
5700          WRITE(6,13)P60(I),W60(I)
5800       21 CONTINUE
5900        5 FORMAT(1X,6(D17.10,5X))
6000        9 FORMAT(45X,4(D17.10,5X))
6100       13 FORMAT(89X,2(D17.10,5X))
6200 C  COMPUTATION OF THE SHIELDING FUNCTION SS(I); THIS FUNCTION IS DEFINED
6300 C  AS THE RATIO BETWEEN THE COUNT RATE WITH SHIELDING EFFECT AND WITHOUT
6400 C  SHIELDING EFFECT
6500 C  GP IS THE GREEK PI
6600 C  READING AND WRITING OF THE DATA CONTAINED IN A.DATAF
6700          GP=3.1415926D0
6800          DO 30 I=1,9
6900          READ(5,40)X(I),Y(I)
7000          WRITE(6,50)X(I),Y(I)
7100       40 FORMAT(D11.4,D10.3)
7200       50 FORMAT(5X,D11.4,10X,D10.3)
7300          X(I)=X(I)*GP
7400       30 CONTINUE
7500 C  COMPUTATION OF THE POINTS (VEKTOR U(K)) IN WHICH THE FUNCTION SS(I)
7600 C  MUST BE EVALUATED
7700          DO 55 I=31,60
7800          K=I-30
7900          UU(K)=P60(I)
8000          U(K)=P60(I)*GP
8100       55 CONTINUE
8200 C  SEE IMSL SUBROUTINES ICSICU AND ICSEVU FOR THE MEANING OF THE
8300 C  SYMBOLS
8400          NX=9
8500          IC=9
8600          M=30
8700          BPAR(1)=1.D0
8800          BPAR(2)=6.D0/(X(2)-X(1))*(Y(2)-Y(1))/(X(2)-X(1))
8900          BPAR(3)=1.D0
9000          BPAR(4)=6.D0/(X(9)-X(8))*(Y(8)-Y(9))/(X(9)-X(8))
9100          CALL ICSICU(X,Y,NX,BPAR,C,IC,IER)
9200          WRITE(6,60)IER
9300       60 FORMAT(10X,I3)
9400          CALL ICSEVU(X,Y,NX,C,IC,U,S,M,IER)
9500          WRITE(6,60)IER
9600 C  PRINT OF THE RESULTS OF THE FITTING PROCESS
9700          DO 70 I=1,30
9800          WRITE(6,80)UU(I),U(I),S(I),I
9900       80 FORMAT(3(10X,D17.10),5X,I2)
10000 C       WRITE(7,90)UU(I),U(I),S(I)
10100 C 90    FORMAT(3(5X,D17.10))
10200       70 CONTINUE
10300 C  EXTENSION OF THE VEKTOR S(I), I=1,30 TO GENERATE THE SYMMETRIC ONE
10400 C  SS(I), I=1,60; PRINT OF SS(I)
10500          DO 110 I=1,30
10600          J=30+I
10700          K=31-I
10800          SS(J)=S(I)
10900          SS(K)=S(I)
11000       110 CONTINUE
11100          DO 120 I=1,60
11200          WRITE(6,130)SS(I),I
11300       130 FORMAT(10X,D17.10,5X,I2)
```

```
11400    120 CONTINUE
11500 C  DATA FOR ASDEX TOKAMAK
11600        A=40.D0
11700        RT=165.D0
11800        DIS=215.D0
11900        B1=5
12000        B2=1
12100        B3=2
12200        B4=2
12300 C  DATA FOR WENDELSTEIN VII STELLARATOR
12400 C      A=3.D0
12500 C      RT=200.D0
12600 C      DIS=118.D0
12700 C      B1=3
12800 C      B2=3
12900 C  REACTIVITY PARAMETERS (GAMOW EQUATION)
13000        A1=3.4920841D-14
13100        A2=20.144728D0
13200 C  DATA RELATIVE TO THE EXPERIMENTAL DETECTING SYSTEM
13300        CHT=1.D-02
13400        EFF=5.9D-01
13410 C   CORRECTING COEFFICIENT FOR THE NEUTRON FLUX, IN ORDER TO USE THE
13420 C   EXACT VALUE
13430         COEF=0.28D0
13500 C  NUMBER OF USED GAUSSIAN POINTS
13600        N=60
13700 C  STRENGTH OF THE PLUTONIUM-BORON NEUTRON SOURCE
13800        Q=6.5D+06
13900 C  SEE IMSL SUBROUTINE ZFALSE FOR THE MEANING OF THE SYMBOLS
14000        EPS=1.E-04
14100        NSIG=4
14200        TEMPL=0.1D0
14300        TEMPR=1.2D0
14400 C  READING AND WRITING OF THE DATA CONTAINED IN A1.SHOT;COMPUTATION
14500 C  OF THE ION TEMPERATURE TIME PROFILE AND PRINT OF THE RESULTS
14600        DO 210 I=1,5
14700        IND=I
14800        READ(5,220)TIME(I),FM(I),DO(I)
14900        WRITE(6,500)TIME(I),FM(I),DO(I)
15000    500 FORMAT(10X,2F9.2,2X,D13.6)
15100    220 FORMAT(2F9.2,D12.5)
15200        ITMAX=40
15300        CALL ZFALSE(FLUX,EPS,NSIG,TEMPL,TEMPR,TAPP,ITMAX,IER)
15400        WRITE(6,200)TIME(I),TAPP,IER,ITMAX
15500    200 FORMAT(10X,'TIME=',F9.2,'  (MS)',10X,'TAPP=',D12.5,'  (KEV)',10X,'
15600       &IER=',I3,10X,'ITMAX=',I2)
15700    210 CONTINUE
15800        STOP
15900        END
16000 C
16100 C
16200        FUNCTION FLUX(TEMP)
16300        IMPLICIT REAL*8(A-H,O-Z)
16400        DIMENSION P10(10),P20(20),P30(30),P40(40),P50(50),P60(60)
16500        DIMENSION W10(10),W20(20),W30(30),W40(40),W50(50),W60(60)
16600        DIMENSION DO(5),FM(5)
16700        DIMENSION SS(60)
```

```
16800       INTEGER B1,B2,B3,B4
16900       COMMON/NCD/P10,P20,P30,P40,P50,P60
17000       COMMON/WEI/W10,W20,W30,W40,W50,W60
17100       COMMON/FIT/DIS,RT,GP
17200       COMMON/FIZ/B1,B2,B3,B4,A1,A2
17300       COMMON/FIL/DC,A,IND
17400       COMMON/FIR/TC
17500       COMMON/FIW/FM,CHT,EFF,C
17600       COMMON/FIC/PN
17700       COMMON/SHI/SS
17710       COMMON/CCR/CCEF
17800       TC=TEMP
17900 C  COMPUTATION OF THE INTEGRAL GIVING PN AND RESULT'S PRINTING
18000 C  AL IS THE UPPER LIMIT OF THE SPACE INTEGRAL
18010 C  AL=A FOR ASDEX
18020 C  AL=10.D0 FOR WENDELSTEIN VIIA
18100       AL=A
18200       PN=0.D0
18300       DO 10 I=1,60
18400       DO 20 J=1,60
18500       PN=PN+FCT(P60(I),P60(J))*W60(I)*W60(J)
18600    20 CONTINUE
18700    10 CONTINUE
18800       PN=PN*(AL/2.D0)*GP
18900 C  COMPUTATION OF THE INTEGRAL GIVING FLUXD
19000       FLUXD=0.DC
19100       DO 35 K=1,60
19200       FLUXD=FLUXD+SS(K)*W60(K)
19300    35 CONTINUE
19400       FLUXD=FLUXD*GP*PN/(2.D0*GP*C*EFF)
19410       FLUXD=FLUXD*CCEF
19500 C  DETERMINATION OF THE MEASURED EXPERIMENTAL VALUE OF THE FLUX
19600       FLUXMD=FM(IND)/(CHT*EFF)
19700 C  THE ZERO OF THE FUNCTION FLUX GIVES THE SEARCHED VALUE OF THE
19800 C  ION TEMPERATURE
19900       FLUX=FLUXD-FLUXMD
20000       RETURN
20100       END
20200 C
20300 C
20400       FUNCTION FCT(R,ALFA)
20500       IMPLICIT REAL*8(A-H,O-Z)
20600       DIMENSION P10(10),P20(20),P30(30),P40(40),P50(50),P60(60)
20700       DIMENSION W10(10),W20(20),W30(30),W40(40),W50(50),W60(60)
20800       DIMENSION DD(5)
20900       DIMENSION SS(60)
21000       INTEGER B1,B2,B3,B4
21100       COMMON/NCD/P10,P20,P30,P40,P50,P60
21200       COMMON/WEI/W10,W20,W30,W40,W50,W60
21300       COMMON/FIT/DIS,RT,GP
21400       COMMON/FIZ/B1,B2,B3,B4,A1,A2
21500       COMMON/FIL/DC,A,IND
21600       COMMON/FIR/TC
21700       COMMON/SHI/SS
21800       AL=A
21900       RX=(AL/2.D0)*(R+1.DC)
22000       ALFAY=GP*(ALFA+1.DO)
```

```
C  VOL IS THE VOLUME ELEMENT
      VOL=RX*(RT-RX*DCOS(ALFAY))
C  DENSITY AND TEMPERATURE SPACE PROFILES FOR THE ASDEX TOKAMAK
      D=D0(IND)*(1.D0-(RX/A)**B1)**B2
      T=T0*(1.D0-(RX/A)**B3)**B4
C  DENSITY AND TEMPERATURE SPACE PROFILES FOR THE WENDELSTEIN VII
C  STELLARATOR
C     D=D0(IND)/(1.D0+(RX/A)**B1)
C     T=T0/(1.D0+(RX/A)**B2)
C  RDD IS THE REACTION RATE ,ACCORDING TO THE GAMOW EQUATION, FOR D-D
C  REACTIONS, NEUTRON BRANCH
      RDD=(0.5D0*D**2)*(A1*T**(-2.D0/3.D0)*DEXP(-A2*T**(-1.D0/3.D0)))
C  FCT IS THE INTEGRAND FUNCTION
      FCT=2.D0*GP*VOL*RDD
      RETURN
      END
```

```
C     B.FIT
C     DATA ARE IN A1.DATA AND A1.DATAF
C     A1.DATA CONTAINS THE GAUSSIAN POINTS AND WEIGHTS
C     A1.DATAF CONTAINS THE EXP. COUNT RATES TO FIT THE SHIELDING
C     FUNCTION
C     THIS PROGRAM PLOTS THE FUNCTION (COUNT RATE WITH SHIELDING AGAINST
C     THE ANGLE BETA) OBTAINED BY INTERPOLATING A SET OF EXPERIMENTAL
C     POINTS. THESE POINTS RELATIVE TO THE MEASURED VALUES OF THE COUNT
C     RATE, WHICH ARE FITTED, ARE PLOTTED TOO
C     FOR A COMPARISON, THE THEORETICALLY COMPUTED (WITHOUT SHIELDING)
C     COUNT RATE IS ALSO PLOTTED
C     SYMBOLS USED:
C     U,S,UX,SY,UXX,SYY FOR THE INTERPOLATED COUNT RATE FUNCTION
C     X,Y,XS,YS,XXS,YYS FOR THE EXPERIMENTAL POINTS
C     CTX,CTY,CSX,CSY,CCSX,CCSY FOR THE THEORETICAL COUNT RATE FUNCTION
      REAL*8 X(9),Y(9),DPAR(4),C(9,3)
      REAL*8 P10(10),P20(20),P30(30),P40(40),P50(50),P60(60)
      REAL*8 W10(10),W20(20),W30(30),W40(40),W50(50),W60(60)
      REAL*8 UU(30),U(30),S(30)
      REAL*8 CTX(32),CTY(32)
      REAL*4 UX(32),UXX(32),SY(32),SYY(32)
      REAL*4 ERX(32),ERY(32)
      REAL*4 XS(11),YS(11),XXS(11),YYS(11)
      REAL*4 CSX(32),CSY(32),CCSX(32),CCSY(32)
      DATA ERX/32*0./
      DATA ERY/32*0./
C
C  READING AND WRITING OF GAUSSIAN POINTS AND WEIGTHS
      READ(5,4)P10,W10
      READ(5,4)P20,W20
      READ(5,4)P30,W30
      READ(5,4)P40,W40
      READ(5,4)P50,W50
      READ(5,4)P60,W60
    4 FORMAT(5D12.5)
      WRITE(6,1)
    1 FORMAT(11X,'P10',19X,'W10',19X,'P20',19X,'W20',19X,'P30',19X,'W30'
     */)
      DO 3 I=1,10
      WRITE(6,5)P10(I),W10(I),P20(I),W20(I),P30(I),W30(I)
    3 CONTINUE
      DO 7 I=11,20
      WRITE(6,9)P20(I),W20(I),P30(I),W30(I)
    7 CONTINUE
      DO 11 I=21,30
      WRITE(6,13)P30(I),W30(I)
   11 CONTINUE
      WRITE(6,15)
   15 FORMAT(////11X,'P40',19X,'W40',19X,'P50',19X,'W50',19X,'P60',19X,'
     *W60'/)
      DO 17 I=1,40
      WRITE(6,5)P40(I),W40(I),P50(I),W50(I),P60(I),W60(I)
   17 CONTINUE
      DO 19 I=41,50
      WRITE(6,9)P50(I),W50(I),P60(I),W60(I)
   19 CONTINUE
      DO 21 I=51,60
```

```
5800         WRITE(6,13)P60(I),W60(I)
5900      21 CONTINUE
6000       5 FORMAT(1X,6(D17.10,5X))
6100       9 FORMAT(45X,4(D17.10,5X))
6200      13 FORMAT(89X,2(D17.10,5X))
6300 C     COMPUTATION OF THE SHIELDING FUNCTION S(I); THIS FUNCTION IS
6400 C     DEFINED AS THE RATIO BETWEEN THE COUNT RATE WITH SHIELDING EFFECT
6500 C     AND WITHOUT SHIELDING EFFECT
6600 C     GP IS THE GREEK PI
6700 C     READING AND WRITING OF THE DATA CONTAINED IN A1.DATAF
6800         GP=3.1415926D0
6900         DO 30 I=1,9
7000         READ(5,40)X(I),Y(I)
7100         WRITE(6,50)X(I),Y(I)
7200      40 FORMAT(D11.4,D10.3)
7300      50 FORMAT(5X,D11.4,10X,D10.3)
7400         X(I)=X(I)*GP
7500      30 CONTINUE
7600         DO 35 I=1,9
7700         XS(I)=X(I)
7800         YS(I)=Y(I)
7900      35 CONTINUE
8000 C     COMPUTATION OF THE POINTS (VEKTOR U(K)) IN WHICH THE FUNCTION S(I)
8100 C     MUST BE EVALUATED
8200         DO 55 I=31,60
8300         K=I-30
8400         UU(K)=P60(I)
8500         U(K)=P60(I)*GP
8600      55 CONTINUE
8700 C     SEE IMSL SUBROUTINES ICSICU AND ICSEVL FOR THE MEANING OF THE
8800 C     SYMBOLS
8900         NX=9
9000         IC=9
9100         M=30
9200         BPAR(1)=1.D0
9300         BPAR(2)=6.D0/(X(2)-X(1))*(Y(2)-Y(1))/(X(2)-X(1))
9400         BPAR(3)=1.D0
9500         BPAR(4)=6.D0/(X(9)-X(8))*(Y(8)-Y(9))/(X(9)-X(8))
9600         CALL ICSICU(X,Y,NX,BPAR,C,IC,IER)
9700         WRITE(6,60)IER
9800      60 FORMAT(10X,I3)
9900         CALL ICSEVU(X,Y,NX,C,IC,U,S,M,IER)
10000        WRITE(6,60)IER
10100 C    PRINT OF THE RESULTS OF THE FITTING PROCESS
10200        DO 70 I=1,30
10300        WRITE(6,80)UU(I),U(I),S(I)
10400     80 FORMAT(3(10X,D17.10))
10500     70 CONTINUE
10600 C    COMPUTATION OF THE THEORETICAL COUNT RATE (WITHOUT SHIELDING)
10700        Q=6.5D+06
10800        EFF=11.012D0
10900        D=226.D0
11000        R=165.D0
11100        DO 75 I=1,30
11200        CTX(I)=(I-1)*GP/29
11300        DS2=(D+R)**2+R**2-2.D0*(D+R)*R*DCOS(CTX(I))
11400        CTY(I)=(EFF*Q)/(4.D0*GP*DS2)
```

```
11500       WRITE(6,85)CTX(I),CTY(I),I
11600 C     WRITE(7,85)CTX(I),CTY(I),I
11700    85 FORMAT(5X,D12.5,5X,D12.5,5X,I2)
11800    75 CONTINUE
11900 C   THE PLOT OF THE FUNCTIONS AND OF THE POINTS IS GIVEN
12000       DO 100 I=1,30
12100       UX(I)=U(I)
12200       SY(I)=S(I)
12300       CSX(I)=CTX(I)
12400       CSY(I)=CTY(I)
12500    100 CONTINUE
12600       CALL PBLATT
12700       CALL PLOTS
12800       STARTX=0.
12900       DELTX=GP/4
13000       ALENGX=11.
13100       AXEINX=11./4
13200       ENDX=STARTX+ALENGX*DELTX/AXEINX
13300       WRITE(6,110)STARTX,ENDX,ALENGX,AXEINX,DELTX
13400    110 FORMAT(5X,5E12.5)
13500       UX(31)=STARTX
13600       UX(32)=DELTX/AXEINX
13700       CSX(31)=STARTX
13800       CSX(32)=DELTX/AXEINX
13900       XS(10)=STARTX
14000       XS(11)=DELTX/AXEINX
14100       DO 120 I=1,32
14200       UXX(I)=UX(I)
14300       CCSX(I)=CSX(I)
14400    120 CONTINUE
14500       DO 125 I=1,11
14600       XXS(I)=XS(I)
14700    125 CONTINUE
14800       STARTY=0.
14900       DELTY=180./3
15000       ALENGY=14.
15100       AXEINY=14./3
15200       ENDY=STARTY+ALENGY*DELTY/AXEINY
15300       WRITE(6,130)STARTY,ENDY,ALENGY,AXEINY,DELTY
15400    130 FORMAT(5X,5E12.5)
15500       SY(31)=STARTY
15600       SY(32)=DELTY/AXEINY
15700       CSY(31)=STARTY
15800       CSY(32)=DELTY/AXEINY
15900       YS(10)=STARTY
16000       YS(11)=DELTY/AXEINY
16100       DO 140 I=1,32
16200       SYY(I)=SY(I)
16300       CCSY(I)=CSY(I)
16400    140 CONTINUE
16500       DO 145 I=1,11
16600       YYS(I)=YS(I)
16700    145 CONTINUE
16800       CALL SKALA(2.,1.,11.,0.,'ANGLE  BETA     (RAD)',21,.2,STARTX,ENDX,
16900      *.2,0.,0,-2.)
17000       CALL SKALA(2.,15.,11.,0.,'BE',0,.2,STARTX,ENDX,0.,0.,0,2.)
17100       CALL SKALA(2.,1.,-14.,90.,'COUNT RATE      (CP)',20,.2,STARTY,ENDY
```

```
17200       *,.2,0.,0,-2.)
17300        CALL SKALA(13.,1.,-14.,90.,'CR',0,.2,STARTY,ENDY,0.,0.,0,2.)
17400        CALL PDATA(2.,1.,UXX,SYY,30,0.,2,0,0,ERX,ERY,2)
17500        CALL PDATA(2.,1.,XXS,YYS,9,0.,0,1,0,ERX,ERY,2)
17600        CALL PDATA(2.,1.,CCSX,CCSY,30,0.,-2,0,0,ERX,ERY,2)
17700        CALL SCHRFT(14.5,15.,.2,'ASDEX TOKAMAK',13)
17800        CALL SCHRFT(14.5,14.,.2,'LITTLE CIRCLES: EXPERIMENTAL POINTS',35)
17900        CALL SCHRFT(14.5,13.,.2,'CONTINUOUS LINE: INTERPOLATED FUNCTION',3
18000       &8)
18100        CALL SCHRFT(14.5,12.,.2,'DASHED LINE: THEORETICAL FUNCTION',33)
18200        STOP
18300        END
```

7. References

/1/ K.H. Beckurts, K. Wirtz, Neutron Physics, Springer-Verlag, 1964

/2/ I.G. Cordey, W.G. Core, The Physics of Fluids, 17, 1626 (1974)

/3/ H.P. Eubank, Neutron Diagnostics, International School of Plasma Physics, Varenna, 1978

/4/ L.M. Hively, Nuclear Fusion 17, 873 (1977)

/5/ D.L. Jassby, H.H. Tower, Nuclear Fusion, 16, 911 (1976)

/6/ G. Lehner, F. Pohl, Zeitschrift für Physik, 207, 83 (1967)

/7/ J.B. Marion, J.L. Fowler, Fast neutron physics, Part I and II, Interscience Publishers, 1960

/8/ G.H. Miley, H. Towner, N. Ivich, Fusion cross sections and reactivities, University of Illinois Report C 00-2218-17 (17 June 1974)

/9/ N. Peyrand, Journal of Plasma Physics, 21, 1 (1979)

/10/ J.D. Strachan, The PLT neutron flux measurement system, PPPL-TM-303, 1977

/11/ J.D. Strachan, A. Bhattacharjee, D.L. Jassby, H.H. Towner, Physics Letters, 66A, 295 (1978)

/12/ H. Eubank et al., PLT neutral beam heating results, IAEA Conference, Innsbruck, 1978

/13/ Equipe TFR, Nuclear Fusion, 18, 1271 (1978)